GEOPRÆVENT AG
Technoparkstrasse 1
8005 Zürich
Tel. 044 419 91 10
Fax 044 419 91 18
info@geopraevent.ch

Technical Report on Measurements of Kleines Nesthorn and Birchgletscher with a Ground Based Interferometric RADAR May/June 2025

Canton of Wallis SDANA

OF1200293.01



Main Contributing Author:

Dr. Johannes Gassner

Zürich, 31 March 2026 / JG

1 Content

1	Content	2
2	Executive Summary	2
3	Introduction	4
4	General Conditions	5
5	Technical Data Summary	7
6	Simulation Results of chosen Radar Location	8
7	Interferograms and Coherence Maps	10
8	GP Adaptive Interferometric Model AIM	14
9	GP AIM Aggregated Results	16
10	GP AIM Riding the Wild Bull	20
11	GP AIM 6- versus 24-Hour Aggregation	23
12	IDS Guardian Results	26
13	DEFOX Birchgletscher Deformation Results	30
Appendix A	Birchgletscher Collapse FlexCam Still Frames	33
Appendix B	Overview Images on Target Area	37
Appendix C	Interferograms and Coherence Maps	42

2 Executive Summary

Between 19 May and November 2025, Geoprevent deployed a ground-based interferometric radar (GBIR) near Blatten Gassun (VS) to monitor the accelerating instability of the east flank of the Kleines Nesthorn and the Birchgletscher during the rapidly evolving hazard situation. Installation coincided with the onset of major rockfalls, which culminated in the catastrophic glacier collapse on 28 May 2025. The chosen location - supported by visibility analyses, resolution simulations, and DEM-based modelling - provided comprehensive coverage of the east, north, and west flanks of Kleines Nesthorn and the upper/lower Birchgletscher.

All results presented in this technical report were obtained a posteriori: they benefit from several improvements relative to the real-time monitoring results available at the time of the event. This re-evaluation and additional post-processing of the data with improved algorithms was agreed upon by the Municipality of Blatten im Lötschental, and its use in *Blatten4Science*[1] was financed by the Canton Wallis SDANA. There are no plans to publish any results from the real-time monitoring.

[1] «Blatten4Science» Research Data of the Nesthorn – Birchgletscher Process Cascade

The radar delivered millimetre-precision deformation measurements but was affected at times by atmospheric turbulence, humidity gradients, snow and the fast surface changes, which caused loss of coherence in the most active zones. Interferograms and coherence maps document a rapidly expanding unstable region, with incoherence on the east flank evident from the beginning of the campaign, consistent with the destructive processes occurring from day one.

The IDS Guardian software provided by the radar manufacturer has proven to be insufficient: velocity estimates saturated at -4 m/day and failed in regions of high deformation rates. To address this, Geoprevent applied the Adaptive Interferometric Model (AIM). AIM adaptively selects optimal interferogram pairs, filters atmospheric artefacts, and allows tracking of velocities up to -14 m/day (median) and locally even higher, significantly expanding the measurable velocity range.

Daily 24-hour AIM aggregations effectively filtered the diurnal atmospheric cycle of the thermally active Lötschental. These results are revealed for the event:

- persistent high velocities on the east flank and distal glacier parts,
- accelerating motion in the glacier front up to the saturation limit at -14 m/day,
- stable behaviour on the north and west flanks.

After the collapse, the focus shifted to slow-movement monitoring to verify the stability of Kleines Nesthorn.

Complementary optical monitoring with a ProCam DEFOX system provided high-resolution imagery. Although pre-collapse changes were too rapid for the application of optical correlation algorithms, the post-collapse analysis confirmed up to decimetre-scale daily motions in the freshly exposed glacier bed.

Overall, the combined radar and optical monitoring strategy delivered, after a posteriori improvement, continuous, high-precision insights before, during, and after the Birchgletscher collapse. The deployment demonstrated both the capabilities and limitations of GBIR in extreme alpine terrain, and it confirmed that advanced processing algorithms (AIM, AIM-RWB, RepeatPass) are essential for achieving reliable deformation measurements in high- and slow-velocity, low-coherence environments. The results provide a uniquely detailed record of the processes leading up to, and following, the 28 May 2025 collapse.

Zürich, 31 March 2026





Dr. Johannes Gassner
Interferometric Radar Expert

Dr. Marc Schneebeli
Geoprevent Team Leader

3 Introduction

Permanent and periodic measurements using ground based interferometric radar (GBIR) are a highly precise and reliable means for determining surface deformations of rock or ice. GBIR measures relative changes in the line-of-sight between the radar device and the terrain surface. This allows identification of deformed surfaces between two measurements at distances of up to 4–5 km. The inherent relative distance resolution of the interferometric radar is 0.1 mm.

The radar's azimuthal resolution is 4.3 mrad, equivalent to a pixel width of 4.3 m at a measurement distance of 1 km. The range resolution of 0.75 m is independent of the distance. Combining the target area slope inclination with the radar's range resolution allows for the addition of height information to every radar pixel and therefore of the surface area covered by the pixel: at 1 km distance it covers thus more than 3.2 m^2 of surface.

The radar antennae used have an opening angle covering 50° in azimuth and 31° in elevation[2]. An interferometric radar can therefore cover a target area of more than 10 km^2 from a safe distance.

The following factors affect the measurement accuracy:

- A stable radar location with good visibility of the potentially unstable area is essential.
- Dry surfaces without vegetation reflect radar signals consistent.
- Atmospheric turbulences during measurements. While large scale atmospheric changes can be mostly corrected for, local changes are the main source of systematic errors: a variation of the relative humidity over 1 km distance by just 1% changes the propagation of the microwaves equivalent to a real deformation of 1 mm.[3]
- Measurement distance: closer range leads to fewer atmospheric disturbances.
- Size of stable areas: the more stable areas around the target zone, the better atmospheric disturbances can be filtered out.
- Snow: some ten centimetres of dry snow are transparent to radar. Once the snow becomes wet, thaws or freezes, the plane of reflection changes and therefore has the same signature as a real deformation.
- Deformations of underlying surfaces can only be detected if snow coverage with constant reflection properties is well connected to the ground and therefore moves together with the surface below.

In summary, GBIR allows the monitoring of a large surface areas with a high precision under most conditions. Depending on systematic effects, mainly produced by atmospheric turbulences, accuracies of 1 mm and better can be achieved in the deformation measurement. Therefore, the radar is affected, but not limited by weather conditions as clouds, precipitation or by day light as are methods based on visible light including cameras and lasers.

[2] Corresponding to the antennas half-power beam width (HPBW)
[3] S. Rödelsperger, "Real-time Processing of Ground Based Synthetic Aperture Radar (GB-SAR) Measurements", p. 15 http://tuprints.ulb.tu-darmstadt.de/2755/



Figure 1: The radar site near Blatten Gassun on the installation day. The radar sensor (yellow) moves along a 2 m long linear scanner. The Peli cases contain electronics, batteries and the fuel cell.

4 General Conditions

The GBIR installation took place on Monday 19 May 2025, when the village of Blatten was evacuated and the Kleines Nesthorn collapsed onto the Birchgletscher. The decision on the location near Blatten Gassun on the opposite side of the Lötschental was based on simulations of various possibilities. It represents a compromise between visibility of the target area, the distance from the target and the in line-of-sight fraction of ground movements (cf. chapter 6).

Figure 1 and Figure 2 show the radar site on the installation day and at the beginning of June. The linear scanner is mounted on heavy concrete blocks to provide stability. The yellow radar head moves along the linear scanner to produce a Synthetic Aperture (SAR) of 2 m in length, providing an azimuthal resolution of 4.3 mrad. The black Peli cases behind the radar instrument contain electronics, batteries and a fuel cell running on methanol.

Until the collapse of the Birchgletscher the radar was powered by a 230V AC land line from a nearby house. After the collapse it was powered by the fuel cell. High temperatures and dry air led to a failure of the fuel cell on 30 May. A tarp provided enough shade from 31 May onward to allow undisturbed radar operation. Solar panels were installed in the beginning of June and thereafter supplied most of the 60 W of power required by the installation.

Data transfer was first provided by GSM. As data bandwidth dropped drastically during night, special priority access was granted by the network operator. A Starlink antenna was installed in June to provide system redundancy.



Figure 2: The radar site after the installation of a tarp, solar panels and a Starlink antenna on 5 June.

Atmospheric conditions are the main source of systematic errors affecting measurements. The first weeks were characterized by frequent precipitation with snow on the upper slopes and rain in the valley. The photos taken with the station radar camera provided an impression of the conditions in the target area. Daily samples are shown in chapter Appendix B in Figure 27 to Figure 29 on page 37ff. Due to the north orientation of the target area the snow on the upper slopes remained until mid-June. In addition, precipitation measurements from nearby MeteoSwiss weather stations[4] are shown in the velocity trends, cf. Figure 10, Figure 12 or Figure 14.

The time needed to move the radar sensor along the linear scanner defines the achievable scan rate. The travel time of the microwaves to and from the target area in 4 km distance limits the speed of the sensor movement. A maximal scan rate of 61 seconds can be achieved for a SAR length of 2 m. A few days after the collapse, deformation velocities had decreased enough to reduce the scan rate and therefore the mechanical wear on the equipment.

[4] MeteoSwiss Open Data Documentation: https://opendatadocs.meteoswiss.ch/

5 Technical Data Summary

GBIR device:	IDS IBIS-FM EVO 2m SAR
Microwave frequency	17.2 GHz ($\lambda \approx 17.43$ mm), 200 MHz Bandwidth
Lateral resolution:	4.3 mrad for 2m SAR length
Spatial resolution @ 3km:	0.75 m (Range) x 13.1 m (Lateral)
Location:	Gassun, Blatten VS, Switzerland
CH1903+ / LV95	2'628'689, 1'141'335, 1’794m, 157°N
Distance to target area	2’700 – 4'000 m
Uncertainty geocoding:	few Meters, manual orientation
Measurement starts:	19 May 2025 12:46 CEST
Operation mode:	permanent
Typical scan period:	61s (May), 121s (June)
Number of scans	14’645 (May), 20’483 (June)
Power consumption:	60 W
Power supply:	230V AC (until 28 May 2025), methanol fuel cell, solar panels (starting from 5 June 2025)

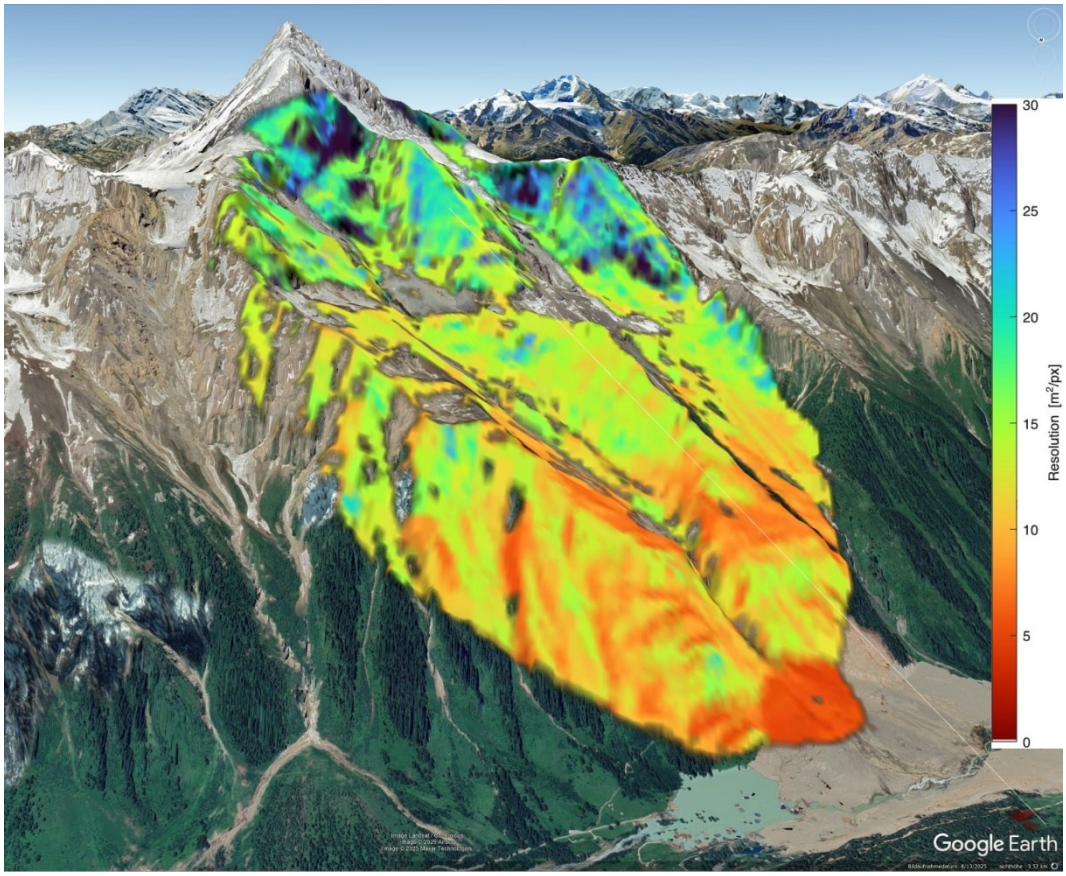


Figure 3: The simulated radar resolution from the chosen location near Blatten Gassun.

6 Simulation Results of chosen Radar Location

Before the installation of the radar several potential sites were considered. The parameters relevant to the decision of the location were, among others:

- coverage of the relevant target area,
- distance to the target area which influences the strength of the radar signal return and the radar resolution in the target area,
- fraction of surface movements visible in line-of-sight to the radar,
- accessibility to the site, energy supply and data communication aspects.

Sites close to the east flank of the Kleines Nesthorn were considered, as well as several potential sites on the valley floor and the opposite side of the valley, e.g. at Weritzstafel, Weissenried and Tellin. Detailed simulations were conducted based on the Digital Elevation Model (DEM) swissALTI3D provided by the Swiss Federal Office of Topography swisstopo[5].

The chosen location near Gassun above Weissenried provides a good coverage of the east, north and west flanks of the Kleines Nesthorn (cf. Figure 3). While the Nestgletscher and the upper Birchgletscher are also well covered, only the front of the lower Birchgletscher was visible from the much lower location near Gassun.

[5] https://www.swisstopo.admin.ch/en/height-models

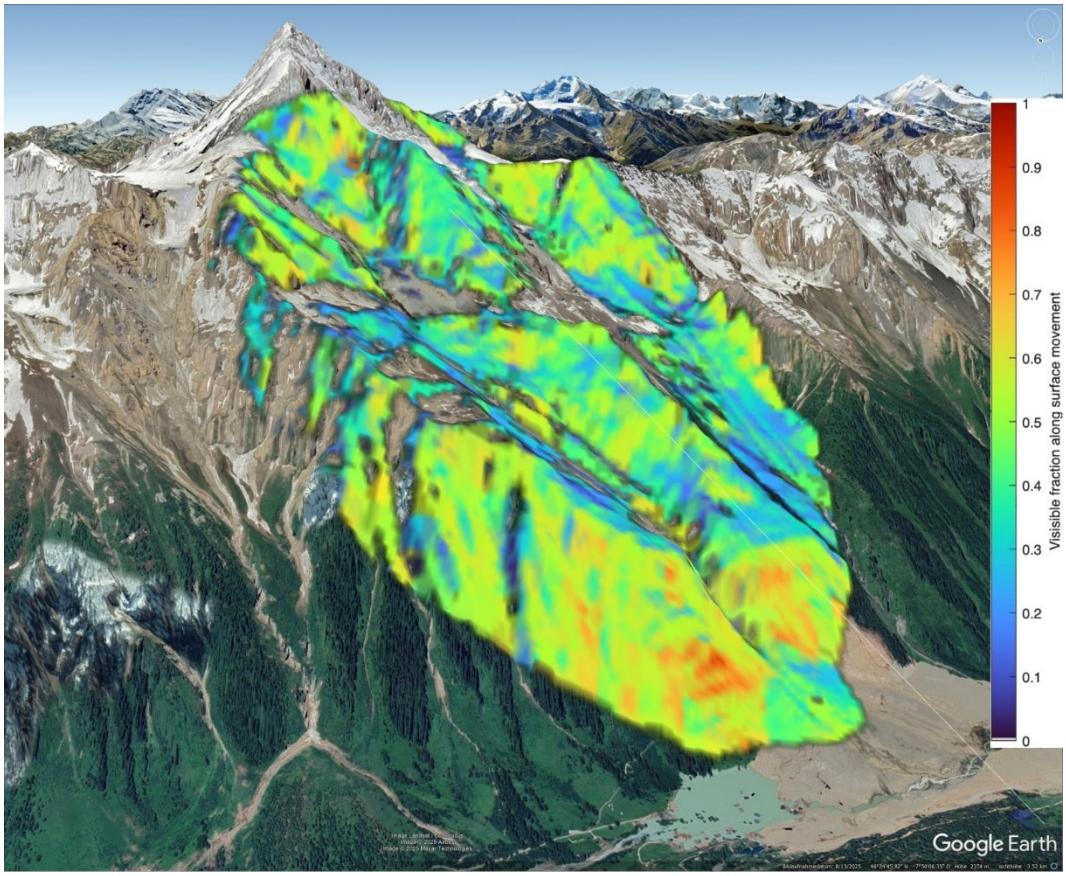


Figure 4: The simulated fraction of gravitational surface movement visible in line-of sight from the chosen radar location near Blatten Gassun.

In the area of the glacier front, a resolution of up the 10 m^2 per radar pixel is achieved from Gassun. On the flanks of Kleines Nesthorn, the resolution decreased mainly due to the sub-optimal orientation of the surface and the larger distance to values of 20 m^2 and more.

A radar site higher up on the opposite slope would have provided a better view of the surface of the lower glacier. The downside of a higher location would have been a greater distance to the target area, and therefore, reduced resolution, less signal return and a lower fraction of gravitational surface movements would have been visible.

The fractions of gravitational surface movements visible in line of sight from the location in Gassun are shown in Figure 4 using Google Earth. On the flanks of Kleines Nesthorn and on the Birchgletscher front, the line-of-sight velocities measured by the radar correspond to more than half of the surface movements following the local gravitational flow vector, which is considered to be sufficient.

The choice of location proved to be advantageous: the blast from the collapse nearly reached the radar site, as can be seen in still frames of the radar site camera shown in Figure 26. The radar installation took no damage at all.

7 Interferograms and Coherence Maps

Interferometric radar measurements are employed to detect terrain displacements with millimetre-level precision. The method involves comparing two data acquisitions to generate interferograms. The left column of Figure 5 and Figure 6 illustrates examples of interferograms from measurements taken prior to, and during the Birchgletscher collapse. The paired radar scans are consecutive and separated by an interval of approximately 61 seconds. Figure 30 and Figure 31 in chapter Appendix C on page 42 show in addition the daily evolution of interferograms and coherence maps up to the glacier collapse.

An interferogram represents the phase differences of two, time separated microwave signals received from the target area. These phase differences range between -π and +π. As the signal path is traversed twice, outbound and return, a phase difference of +π signifies a shift by one quarter of the radar wavelength towards the radar (pixels rendered in red), −π means a shift by λ/4 away from it (pixels rendered in blue). Only the displacement component along the radar line of sight is captured.

The phase difference can be converted into a physical deformation using the radar wavelength λ = 17.43 mm. The maximum unambiguous displacement measurable between two acquisitions is ±λ/4, which equates to ∓4.36 mm (negative values indicating motion towards the radar reducing the distance between target area and sensor, positive values indicating motion away from it).

Large-scale atmospheric variations are corrected by comparing the two measurements within stable areas. Since, by definition, no deformation occurs in these zones, a robust second-degree, two-dimensional polynomial fit is applied and subtracted from the raw data. The quality of this correction can be assessed by the residual of the fit: it ranges between 0 and π and, for this site, typically varies from 0.4 to 0.8 for interferograms with a 5-minute time base.

Within the monitoring area, the radar relies on a largely unchanged surface across its entire field of view to enable accurate comparison of successive measurements. The observed surface and its reflective properties must remain stable; significant changes can impair measurement quality. Such changes may result from construction activities, erosion or precipitation.

A key metric for assessing these changes is data coherence, which ranges from 0 (completely incoherent) to 1 (perfectly coherent). The right column of Figure 5 and Figure 6 presents examples of coherence corresponding to the interferograms on the left. Coherence remains high (represented by yellow tones) in stable areas, whereas it is lost in vegetated or sliding zones within a short period (represented by blue tones).

The surroundings of the target area exhibit low coherence at places. These low coherence zones are caused mostly by vegetation and trees, which diffusely reflect microwaves. They also change according to external conditions, like precipitation or wind which causes vegetation movement.

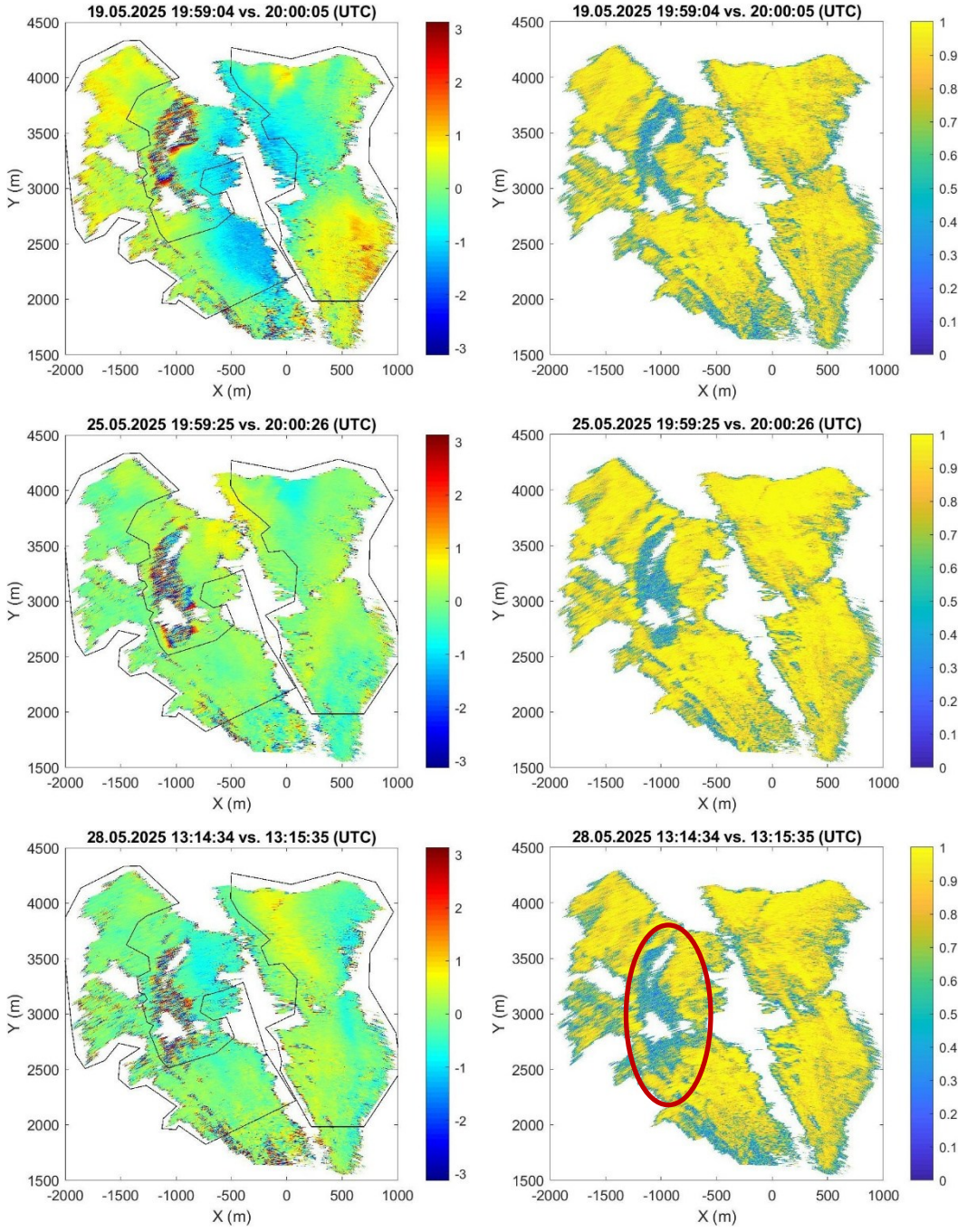


Figure 5: Interferograms (left) and coherence maps (right) of consecutive scans during phase 2 from 19 to 28 May 2025: Rockfalls up to catastrophic glacier collapse. The lower Birchgletscher and Kleines Nesthorn east flank area is indicated with a red ellipse. The axes are in radar coordinates.

The coherence immediately after the installation on 19 May 2025 (upper row in Figure 5) was generally good. Clearly visible is the area of the collapse on the East flank of the Kleines Nesthorn though: The interferogram shows colourful patterns and the coherence values are below 0.6. This is a clear sign for an incoherent, i.e. spatial inconsistent deformation in the area right from the beginning of the measurements.

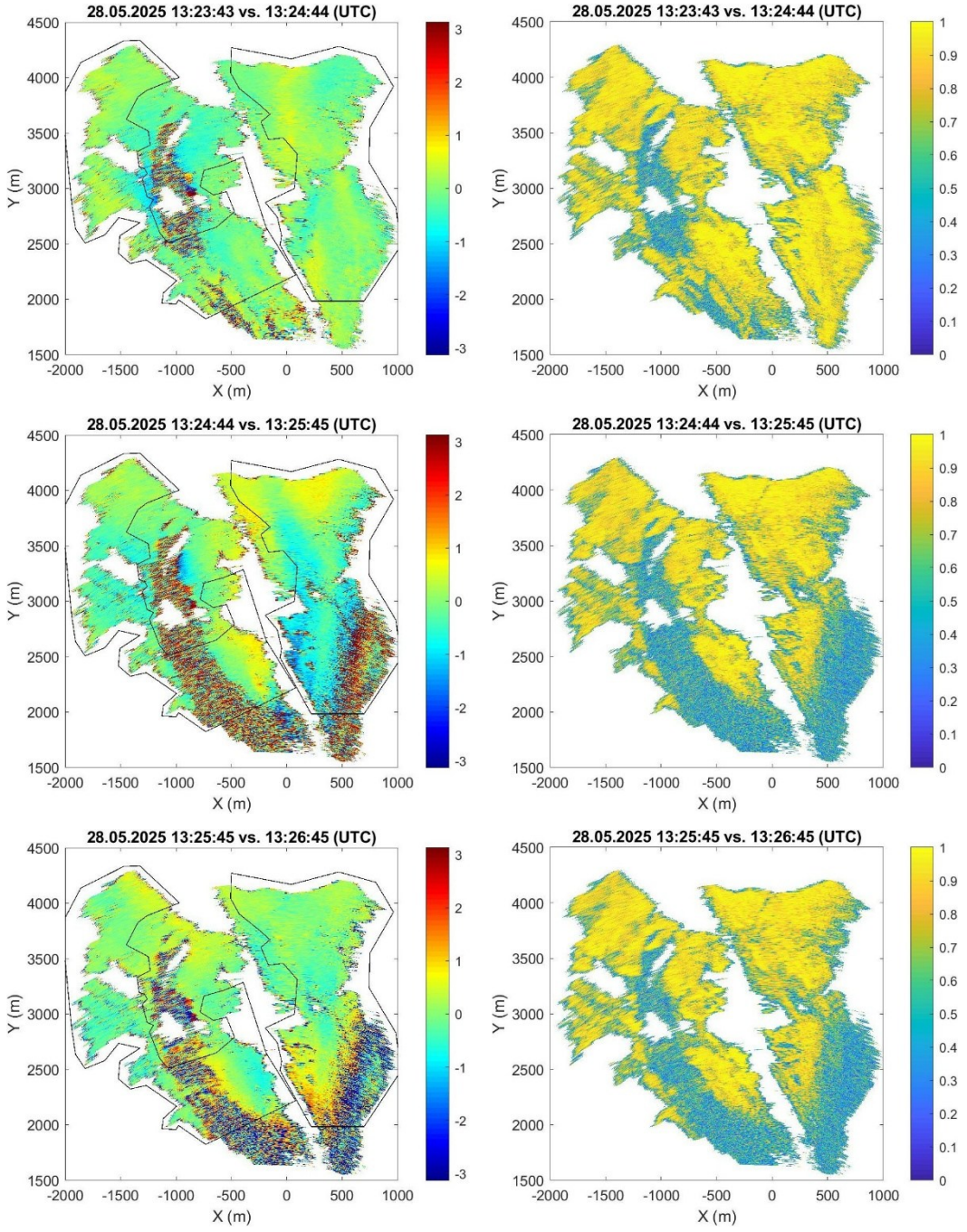


Figure 6: Interferograms (left) and coherence maps (right) of consecutive scans during the glacier collapse on 28 May 2025 at 3:25pm local time.

The incoherent area expands with time: on 25 May (2nd row in Figure 5) the front of the lower Birchgletscher has also become incoherent. The last row and Figure 6 show the interferograms and coherence distributions during the collapse. The path of the debris through the Birchbach valley becomes clearly visible. The lateral extension of the blast also disturbed the radar results in the adjacent areas at lower altitudes, especially in vegetated areas.

Even though coherence may be conserved over a short period, e.g. the time between consecutive scans, it might be lost, when covering longer periods. This

becomes important, e.g. when areas with slower velocities are studied, as interferograms with a longer time base have a better velocity resolution. In summary, deformation measurements using GBIR depend on the relevant velocity range, which dictates the length of the time separation to be considered and if the coherence is conserved over this period.

All the plots in Figure 5 and Figure 6 are shown in radar coordinates, which use the distances and horizontal azimuthal angles measured by the radar. As the vertical elevation angle is not measured, radar coordinates cannot be transformed directly into Cartesian coordinates. Therefore, results in radar coordinates are not suitable to be overlain directly on an orthographic map.

A transformation into real world coordinates is possible for most points with the help of a DEM. As the distance and the horizontal azimuth angle is measured by the radar, the vertical elevation angle can be deduced by intersecting the surface of the DEM with the corresponding radar range gate around the radar site: usually there is only one point on the DEM at the correct distance in the corresponding azimuthal direction, even though ambiguities cannot be excluded.

As previously stated, coherence is the most important quality measurement to judge the reliability of the interferometric radar deformation result. Coherence was lost in all relevant areas either at the onset, or during the event's progress. This indicated that the process was too fast to be tracked reliably with the interferometric radar.

This explains why the industry standard analysis of IDS, the Guardian software, was unreliable in some areas from the beginning of the event. Even though the theoretical velocity range limit is ±6.4 m/day for the measurement settings, the velocity values measured in the corresponding Regions of Interest (ROIs) saturated at values of -3.9 m/day and showed unreasonable values in the higher velocity areas for this analysis approach. This is due to phase wraps at higher speeds which systematically distort the measurement results.

As explained in the next chapter, Geoprevent developed a method to track the event progress at much higher velocities: -14 m/day are observed as a saturation limit for the median in the ROIs and -20 m/day for the 1st percentile (AIM), respective -36 m/day for a special analysis approach (AIM-RWB). To achieve results for such high velocities, the quality requirements on the coherence in the affected areas were lowered, especially for components corresponding to the phase difference: the coherence values in the very fast areas are mainly based on the amplitude distribution of the received signals alone.

The drawback of this special treatment is the reliability of results in these regions with high velocities is difficult to evaluate, as such, they should be treated with great caution.

The results shown in this technical report are achieved with improvements developed after the Blatten event. While they were not available at the time of the Blatten event itself, they are now available also for real-time monitoring and proofed consistent with other measurement methods for the Brienz/Brinzauls (GR) event in November 2025.

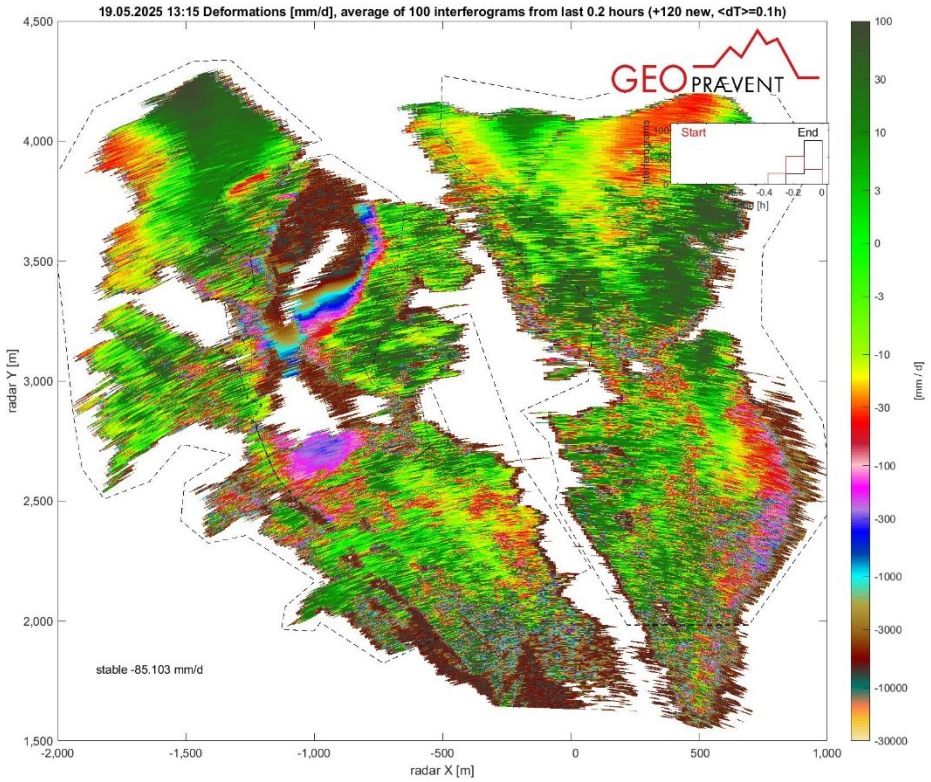


Figure 7: The running average over the last 100 selected interferograms is the most reactive result of AIM to cover short term developments of the monitored area. The information given in the plot are explained in detail inside the text.

8 GP Adaptive Interferometric Model AIM

Monitoring landslide-prone areas in an alpine setting places unique demands on the analysis of GBIR measurements. For this reason, Geoprevent developed the “Adaptive Interferometric Model” (AIM), which is better suited to such conditions than the Guardian standard evaluation model, offered by the radar manufacturer IDS, which is primarily used in open-pit mines.

AIM is based on the core idea of selecting the most suitable pairs of radar measurements from the vast number of possible combinations of two temporally separated acquisitions, focusing on those with the most favourable atmospheric conditions. In addition to the quality of atmospheric correction, an adaptive model is applied that considers the recent history of conditions in the monitored area.

The AIM analysis is computed in batches four times per hour. All measurements from the past 15 minutes are compared with preceding measurements. Suitable pairs are added to a running average comprising over 100 interferograms. Figure 7 shows one of the first result after the installation on 19 May 2024.

The results from the 100 interferograms are primarily technical in nature and should only be interpreted by trained experts. The result is presented in local radar coordinates with the radar positioned at the origin and aligned along the Y-axis. Deformation is encoded according to the colour scale shown on the side, where negative deformation values indicate movement towards the radar. The logarithmic colour scaling allows visualization of a large velocity range with constant relative differentiation, i.e. the number of colour changes per magnitude stays the same. This reflects the possibility of the algorithm to resolve four orders of magnitude, starting at millimetres and ending at 30 metres per day.

The title in Figure 7 specifies the end time of the analysis in local time. It also states that the running average comprises 100 interferograms, with the second, later measurement taken within the last 0.2 hours. The numbers in brackets indicate that 120 new interferograms were added for the current evaluation, and the average time interval of the interferograms <dT> is 0.1 hours.

The distribution in the upper right corner shows the histogram of the relative start and end times of the interferograms used, expressed in hours before the analysis end time, thereby enabling a better interpretation of the timeliness of the radar result displayed.

In the lower left corner, the mean deformation within the stable areas is given with -85 mm/day. The potential stable areas are shown in the plot with dashed lines. Inside these areas the AIM algorithm dynamically determined the radar pixels used for the atmospheric corrections. This rather large value reflects the great variations seen in the large area covered by the stable area: it includes glaciers as well as forests and other overgrown or snow-covered parts of the mountain. It indicates the importance of the outlier rejection performed in the atmospheric corrections.

The area with high velocities is surrounded by dash-dotted lines. As explained in section 7 the coherence criteria are relaxed in this area to cope with the occurrence of very fast movements. Early deformations of -10 m/day (maroon to pine green colours) and over, were measured on the east flank of Kleines Nesthorn. These values represent most likely only a lower velocity limit as the collapse of the mountain was already in full progress. In this early phase of the event, it was crucial to monitor in addition to velocities and accelerations also the extent of the disintegrating area, indicated in Figure 7 by the front with many colour changes.

The quarter-hourly results serve as guidance and support for trained experts in making timely assessments during rapid changes. They should always be considered in the context of the diurnal cycle to evaluate thermal influences (cf. next section). Furthermore, the results should be checked for timeliness using the histogram distribution. If no suitable new interferograms are found within a given period, no result is displayed for that period.

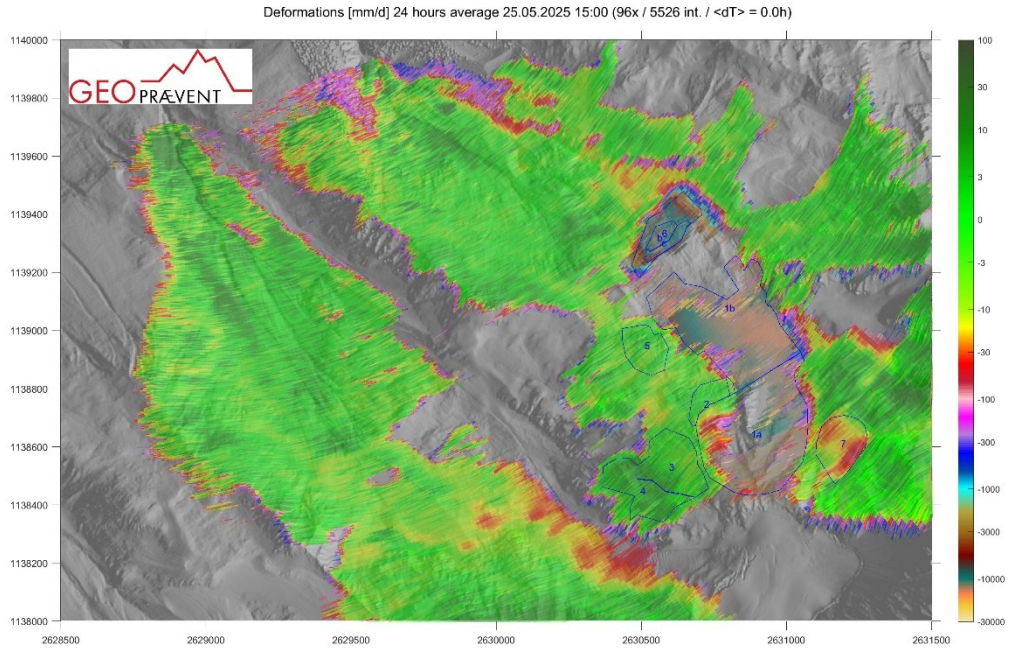


Figure 8: The AIM results aggregated over 24 hours before 3pm on 25 May are shown projected onto an hillshade map. The ROIs are drawn with blue lines. Further information given in the plot are explained in detail in the text.

9 GP AIM Aggregated Results

The 100 interferogram average process, discussed in the previous chapter is prone to atmospheric disturbances. This is especially true for Kleines Nesthorn, which is located close to the main Alpine ridge. The Lötschental and in general the Valais main valley is known to be one of the thermally most active areas in Europe. During daytime thermally activated air masses rise in these high Alpine regions. The following air masses from the pre-Alpine flats, which are pulled through the downslope valleys leading to the main valley, reach wind speeds of 40 km/h and have a high-water content. This leads to artefacts in the radar results. In the second part of the night this process reverses and humid, cold air masses sink along the mountain slopes. This leads to dew and frost formation which also disturbs the sensitive radar measurements.

A change of only 1% in relative humidity along 1 km of the microwave path corresponds, as already stated in section 3, to an apparent displacement of about 1 mm. The radar waves need to propagate more than 7 km on their way to and from the active zone on Kleines Nesthorn. It is therefore not surprising that the radar results can show significant systematic effects on a short term in the diurnal cycle, especially on days with strong solar radiation.

AIM makes it possible to filter out turbulent atmospheric conditions very effectively, such as ascending or descending air masses in the atmosphere caused by thermal activity or wind. However, the radar cannot determine whether a measured deformation is due to an actual landslide or a local, temporal change in atmospheric conditions.

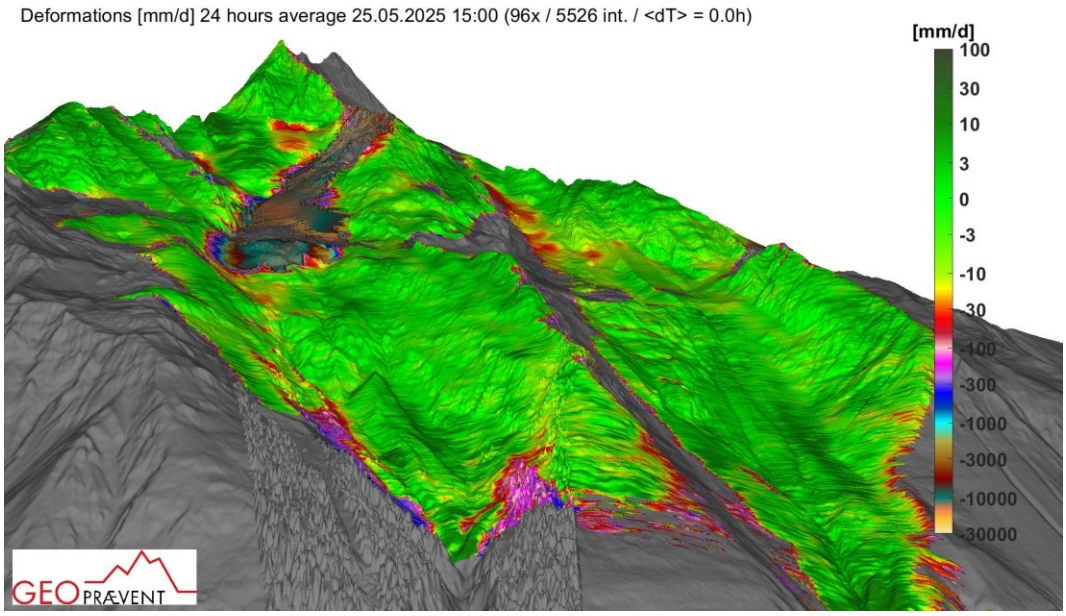


Figure 9: The same results as in Figure 8 are shown projected onto the DEM relief. Further information given in the plot are explained in detail in the text.

From these explanations follows the need for results that reliably filter out the diurnal atmospheric cycle. The AIM aggregates measurements over a certain period to achieve this goal. Figure 8 shows the AIM 24-hour result on the afternoon of 25 May overlayed on an hillshade map, Figure 9 shows the same data projected onto the topographical relief. The very precise DEM used for the projection was recorded by TERRADATA two days before on 23 May. Coordinates are in CH1903+/LV95.

The distributions shown in the figures represent the most probable deformation values within the current day. The header specifies the central date of the measurement in local time. It also indicates in brackets how many quarter-hourly results (96×) were used for the aggregation, the total number of interferograms included (5526 int.), and the mean temporal spacing of the interferograms <dT> which was less than 0.1 hours. To clearly identify a deformation, movement across at least 3 × 3 pixels is generally required, which corresponds to 100 m² or more in the core area of the landslide.

The aggregation eliminates most of the systematic atmospheric effects. Therefore, this representation is easier to interpret for a broader user group. At this stage of the event the measurements on the east flank were already in saturation at about -14 m/day, which were shown in the coral colour for days. The Birchgletscher front reached this saturation point at some places, while the majority of points still have values around -10 m/day (pine green).

ROI 7 in the east of Kleines Nesthorn, shown in the DEM projection on the left of the collapsing flank, contains the upper part of the Birchgletscher, which is visible from the radar site. In May, a mostly continuous flow of about -3 cm/day is measured (red colour). In June, the diurnal freeze-thaw cycles become more accentuated due to the higher position of the sun and the generally warmer conditions.

Only a small part of the Nestgletscher on the west side of Kleines Nesthorn is visible from the radar site as a red strip indicating similar velocities. It shows the similar behaviour as the upper Birchgletscher. At lower altitudes, trees moving in the wind lead to apparent movement artefacts in magenta and blue.

The theoretical accuracy of AIM velocity measurements is better than 1 mm/day. Interferograms with a large time interval allow precise determination of deformation: for example, a time difference of dT = 2 hours enables an accuracy of approximately 1 cm/day in a single interferogram. However, such an interferogram can only resolve velocities unambiguously within a range of ±5 cm/day (see Section 7). Conversely, interferograms with short time intervals allow clear measurement of higher velocities: a time difference of dT = 61 seconds resolves a velocity range of ±6.4 m/day, but only with an accuracy of about 2 m/day.

AIM combines the advantages of short- and long-interval interferograms, achieving high accuracy (up to 1 mm/day) across a wide velocity range (over -14 m/day possible). By averaging dozens of interferograms for the quarter-hourly results and typically several thousand for the 24-hour results, statistical errors are reduced, in best case scenarios, by a factor of 100. Under optimal conditions this enables deformation accuracies of up to 1 mm/day. However, these accuracies do not account for systematic effects, which are mainly caused by changes in atmospheric conditions (see also Section 7).

The extension of the theoretical velocity range of ±6.4 m/day is achieved on one hand by shifting the phase differences to cover an asymmetric range, e.g. shifting by π/2 can cover the range between [+3.2, -9.6] m/day. Such a procedure was applied in the online analysis during the event and allowed a tracking of velocities up to -10 m/day.

On the other hand, an additional phase wrap tracker was developed offline to follow the first phase wrap in the high velocity areas. Such a phase wrap tracking is only possible though if the acceleration process is continuous. Especially for the glacier front, the development contains many discontinuities, mainly at the last stage of phase 2, when parts of the glacier front broke away piece by piece. Nevertheless, the approach allowed extension of the velocity range of up to -14 m/day for the median values inside the affected ROIs. Higher real velocities either saturate at the value itself or are systematically shifted (one phase length translates into a 12.8 m/day shift for the shortest interferograms).

Figure 10 shows the median velocity trends inside the ROIs based on the AIM 24-hour results, which are shown for first phases of the event until the collapse on 28 May. Most parts of the collapsing east flank (ROI 1a in magenta) have already been in saturation at the onset of the radar measurement on 19 May. The distal part of the lower Birchgletscher tongue (ROI 1b in brown) showed velocities of -4 m/day at the beginning and saturated latest on 25 May. These trends are unreliable as the collapse of the east flank did neither happen continuously nor in chunks large enough to be resolved by the radar resolution.



Figure 10: The median velocity trends inside the ROIs based on the re-processed AIM 24-hour results are shown for the 2nd phase of the event until the collapse on 28 May (scale on the left y-axis, see text for detailed discussion). The yellow curve represents the 24-hour precipitation sum measured by the MeteoSwiss weather station in Blatten (scale on right y-axis).

The velocity of the Birchgletscher front (ROI 6 in dark violet, ROI 6b in cyan and ROI 6c in light violet) was first measured around -25 cm/day. After the mass of the collapsed east flank was deposited on the Birchgletscher, the front of the glacier accelerated continuously, until the measurement saturated on 25 May at -14 m/day. While the trend looks feasible up to this point, the flat (or even decelerating) part thereafter represents a saturation limit for higher real velocities.

ROI 2 (Red) is positioned adjacent to the collapsing east flank toward the north side of the mountain. It showed velocities of about -65 cm/day at the start of the radar measurement. The region then decelerated during the first days and remained stable after 21 May.

ROI 3 and 4 cover the east flank of Kleines Nesthorn. Fortunately, this side of the mountain remained stable and exhibited velocities close to zero. ROI 5 was a reference area on the side of the Birchgletscher front which also stayed compatible with zero for the whole time.

In addition to the velocity trends, Figure 10 also contains the precipitation sum of the MeteoSwiss weather station in Blatten. At the altitude of the Birchgletscher the precipitation occurred as snowfall which distorted the radar measurements slightly. The effect was not considered to be significant though.

A possibility to increase the resolvable velocity range is to shorten the SAR length of the radar and therefore reduce the scan time, e.g. by halving the SAR length to 1 m the scan period drops by a third to about 40 seconds per scan. This allows to increase the velocity range by a third. The saturation velocity for Blatten could have

been increased to about -20 m/day. Considering the accelerations this increase would have covered some additional hours for the glacier front.

There are two disadvantages of such a scan length change though: first, the reduced SAR length leads to a decrease in the azimuthal angle resolution, i.e. a 1 m SAR length resolves only 9.7 mrad and therefore more than doubles the area covered by one radar pixel. Secondly, all AIM models must be completely re-trained. The re-training typically takes 12 to 24 hours, during which no radar results are available. Even though the results can be reprocessed offline after retraining, the system is initially blind during this time. A switch is possible with only little down time, if such an option was initiated beforehand. Such preparations were not possible in case of the Blatten event.

10 GP AIM Riding the Wild Bull

In theory it should be possible, to track more than one phase wrap. Therefore, another phase unwrapping approach was developed in the aftermath of the Blatten event. This “Riding the Wild Bull (RWB)” variation does not shift the range of the phase difference but tries to follow each phase wrap by tracking the acceleration of each point. If a measurement approaches the limit of the range, e.g. a phase difference close to +π, but the next measurements show consistent negative values close to -π, a phase wrap is assumed, and the phase difference is corrected by adding a factor of +2π to the phase difference. This procedure is applied for both, accelerations as well as decelerations.

The situation in Blatten was not optimal for such an approach: the unwrapping can succeed only, if the (de)acceleration processes are continuous and the increase in acceleration is slow enough to be tracked properly. Additionally, an unobstructed view of the full moving area, and in line-of-sight motion are an advantage. Such a situation can be found e.g. for the GBIR monitoring of the slide in Brienz/Brinzauls (CH), where the events of June 2023 and November 2025 showed also very high velocities.

In Blatten only the front of the Birchgletscher was clearly visible from the radar site. The surface of the lower Birchgletscher was mainly hidden and only portions of the distal glacier could be seen. Both visible parts were very active during the event. On the distal sections of the glacier, a constant flow of debris from the east flank continued throughout, and after the collapse. Such violent transport and deposition processes morphologically distorted the surfaces along the path of the falling debris. This destroyed the coherence and rendered radar measurements impossible.

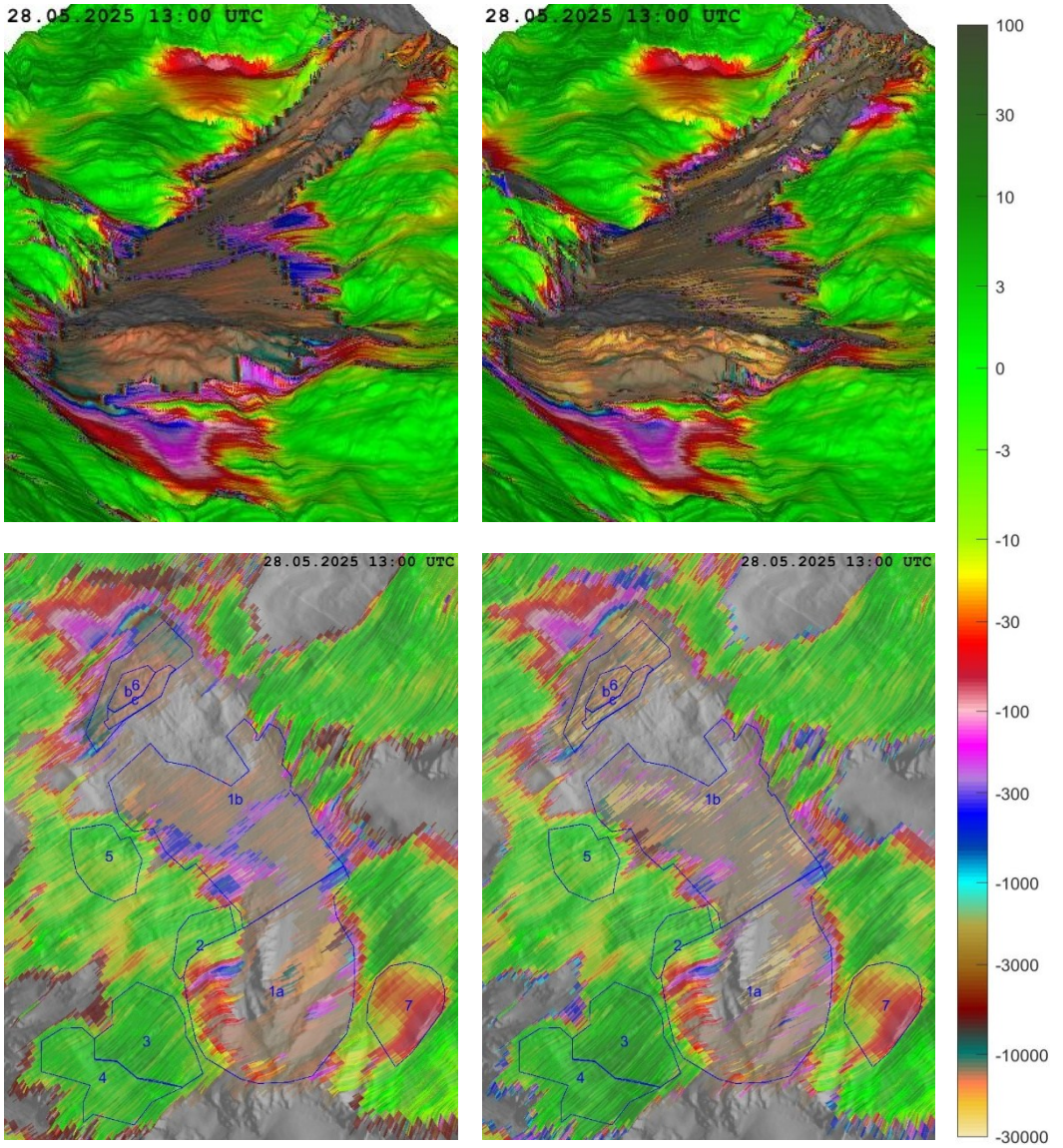


Figure 11: The results of the standard AIM (left column) and the AIM-RWB phase unwrapping approach (right column) are compared for the results at 3pm on 28 May. Only the most active zone is shown on the DEM (upper row) and a hillshade map (lower row).

Nevertheless, as an example, results of the AIM-RWB approach are compared shortly before the collapse to the AIM standard approach in Figure 11. The standard approach in the left column is, for nearly the full active zone, in saturation at about -14 m/day (Coral colour). The AIM-RWB shows a very similar saturation. Therefore, median values in the corresponding ROIs are nearly identical. Locally, there are some differences though, which might be of interest. As expected, the AIM-RWB shows in certain parts even higher velocities in saffron and vanilla colours. Velocities of up to -37 m/day towards the radar were recorded, especially on the sides and top of the Birchgletscher front and at the distal part of the glacier tongue. While these values are probably closer to reality, they are not consistent or reliable enough to give a much clearer picture of the event.

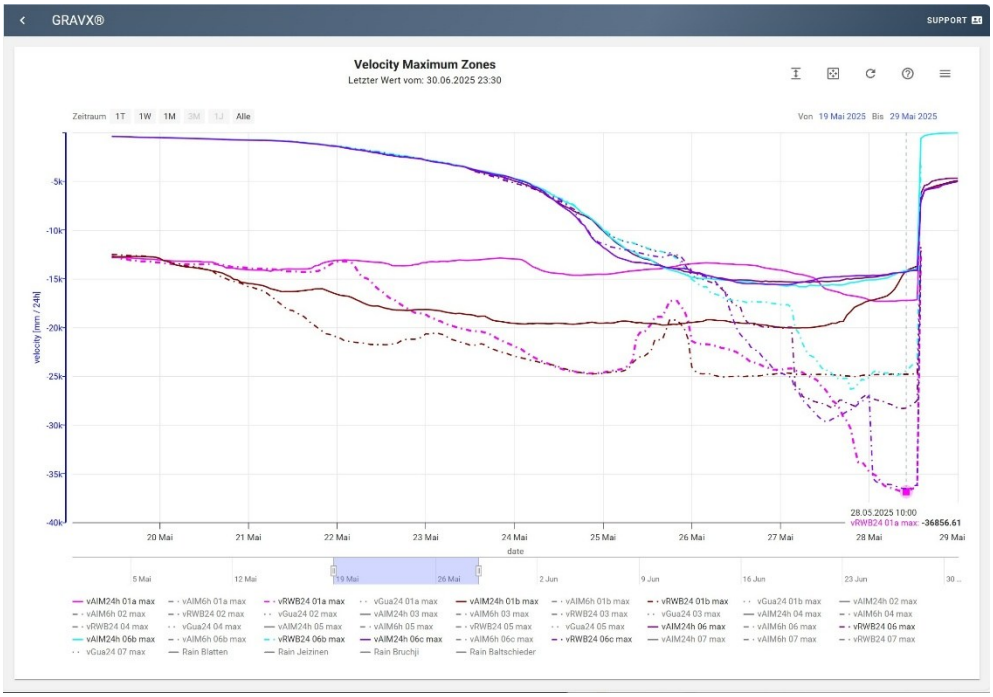


Figure 12: The 1st percentile maximum velocity trends inside the ROIs are shown for 2nd phase of the event until the collapse on 28 May. The standard AIM approach (solid lines) is compared to the AIM-RWB approach (dash-dotted lines).

While the difference between the two approaches is negligible in the ROIs' median values, the trends of the extrema inside the ROIs show clear differences. In Figure 12 the velocity maxima trends are shown for the regions most affected by the collapse. The velocity maxima are determined by the 1st percentile inside the ROI, i.e. 1% of the radar pixels inside the ROI are even faster than the value given. This definition leaves some room for outliers and is therefore more robust than an absolute extremum inside the ROI.

The velocity maxima reached on 28 May was about -37 m/day on the east flank (ROI 1a). A rather flat curve at about -25 m/day is observed for the distal part of the Birchgletscher (ROI 1b). The coherence in the latter observation was low during the whole period up to the collapse as high debris volumes from the east flank hit the area.

The full front of the Birchgletscher (ROI 6) was also measured at approximately -28 m/day for the last hours before the collapse. The smaller section of the lower front (ROI 6b) shows slightly lower extreme values of around -26 m/day, while the upper front reaches, towards the end of the event, values close to -37 m/day.

This approach provides only limited additional insights, as real velocities probably were higher still (cf. ProCam image analysis in chapter 13). The trends also include some sudden steps indicating the fundamental problem of the attempt: due to the disruptive character of the process, an approach relying on continuous, slow changes, is supposed to fail.

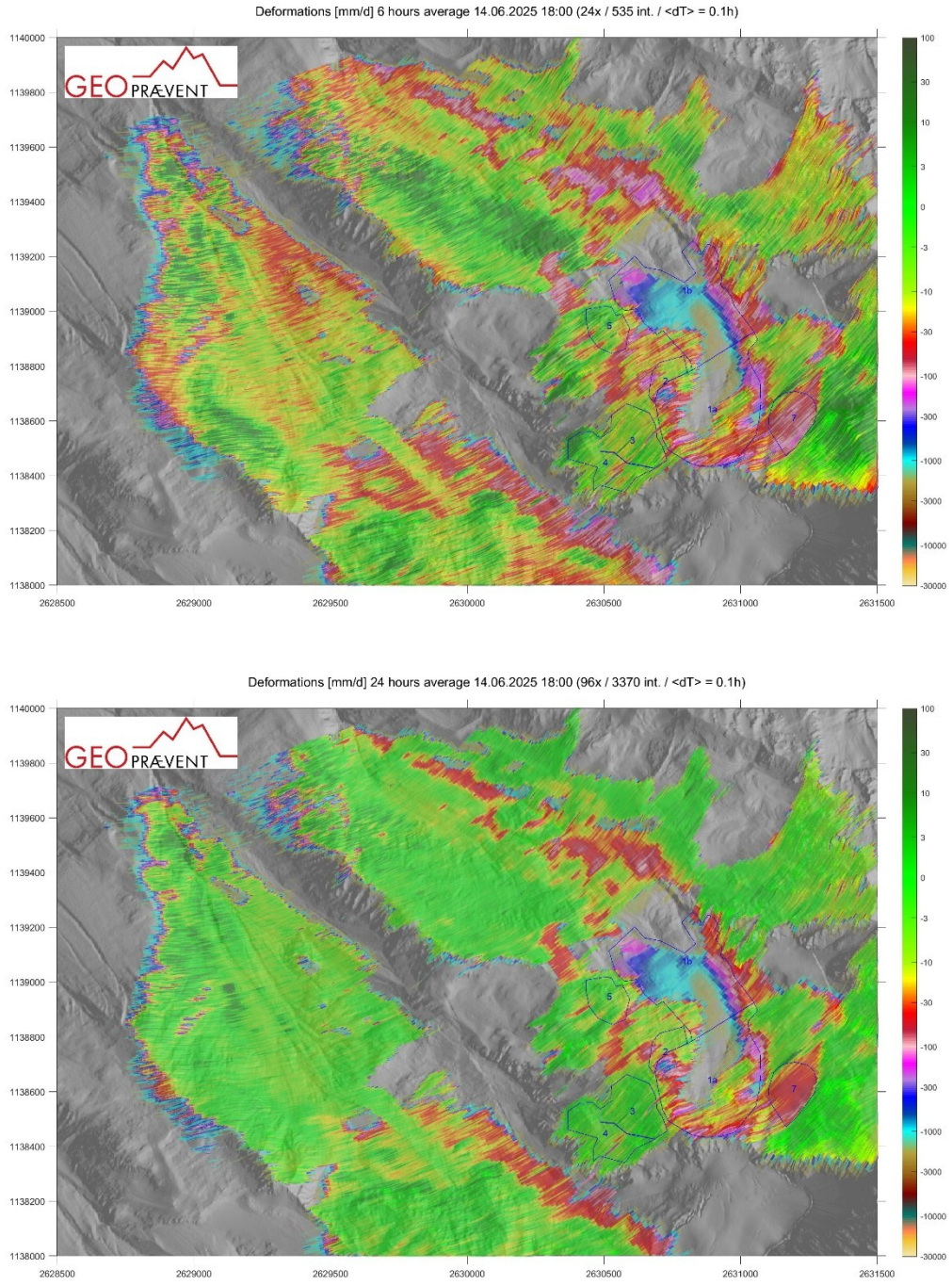


Figure 13: The results of an aggregation over the AIM results of 6-hour (upper) are compared with the 24-hour aggregation (lower) at the end of 14 June, a day with very labile atmospheric conditions.

11 GP AIM 6- versus 24-Hour Aggregation

In the former chapters the need for aggregating AIM results over a longer period was shown to be very sensible. The approach unfortunately introduces an artificial delay into the reactivity of the results. As the aggregation shows only the most probable value of the period, changes might need as long as half the period to influence the results.



Figure 14: The results of 6-hour and 24-hour AIM aggregations are compared for three representative ROIs during the extremely hot June 2025. The daily cycles are most clearly visible for the melting and freezing upper Birchgletscher (ROI 7 Brown). The 24-hour precipitation from the MeteoSwiss weather station in Jeizinen is also shown.

An average over a full day period allows a good compensation of the diurnal atmospheric cycle but introduces a time lag of 12 hours. Such a lag is undesirable in the online monitoring. Therefore, an average of only 6 hours was mostly used as this is a compromise between atmospheric artefacts and reactivity during the event.

The impact of a shorter aggregation period is shown in Figure 13 at the end of 14 June, a day characterized by unstable atmospheric conditions with thermal activity, thunderstorms and little rain in the target area. While the differences in the areas where high velocities persisted are negligible, the stable areas show deformations of up to several cm/day. These can be triggered by surface material and gravel mobilized by rain, e.g. in the channel of Birchbach. In forests rainfall can also appear as artificial deformations.

Figure 14 shows median trends in some representative ROIs for the full month of June 2025. This month was very hot with periods of unstable atmospheric conditions and thunderstorms. Therefore, the diurnal cycles were quite pronounced as can be seen for the dashed curves representing the 6-hour aggregations in selected ROIs. When these trends are compared with their corresponding 24-hour results (solid lines), the smoothing effect of aggregating over a full day cycle becomes clearer.

The best example for the smoothing effect of the 24-hour aggregation is seen for the upper Birchgletscher in ROI 7 (Brown): due to the high position of the sun in June, the glacier was exposed to direct solar radiation. This factor combined with high temperatures led to significant rates of snow melt during the daytime. At night, the surfaces refroze, temporarily limiting the daytime melt effect. This melt-freeze cycle changes the reflection plane for the radar measurements: while the

microwaves can penetrate several centimetres of dry snow, they reflect on a wet surface layer. These variations lead to the diurnal fluctuations in the measured deformations of several centimetres seen in Figure 14.

The collapsed east flank and the glacier bed were filled with gravel, soil and fine sediment. As a result of local precipitation, there were still significant mobilization, transport and deposition processes occurring, increasing the process rates of the unconsolidated material, which can be better observed for shorter aggregation periods.

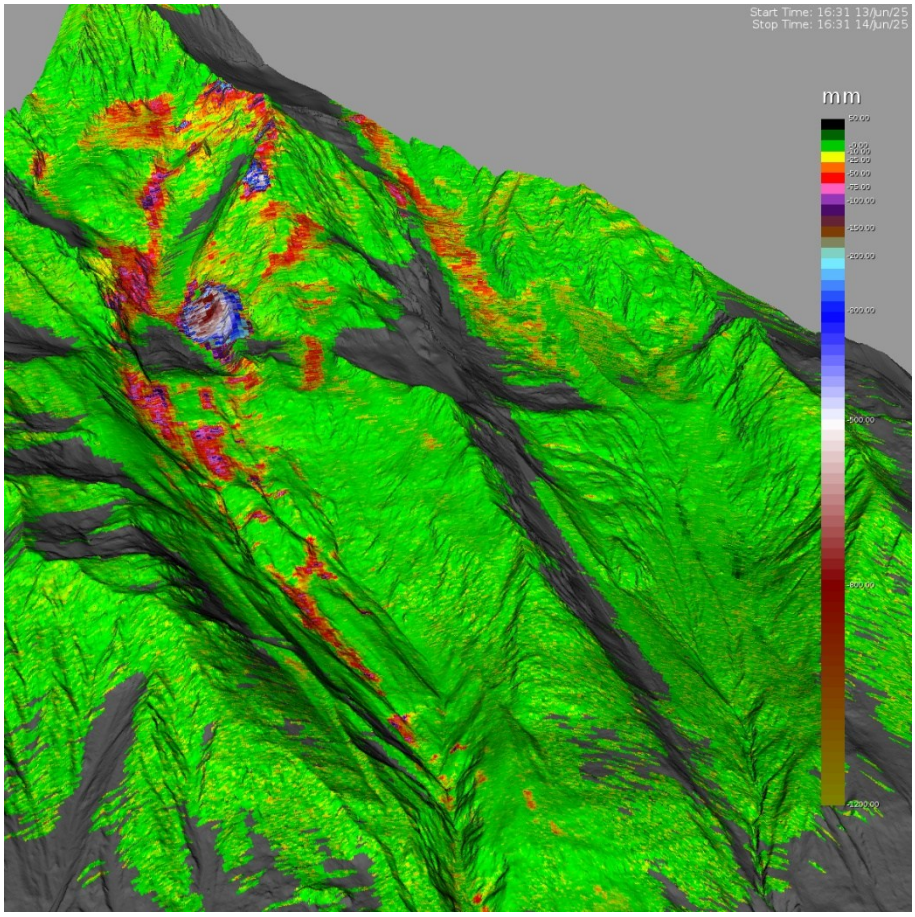


Figure 15: An example of a Guardian 24-hour deformations result from mid-June is projected on the DEM relief. The result is directly produced by the Guardian SW and uses a linear and not the logarithmic colour scale applied to all AIM results.

12 IDS Guardian Results

The radar manufacturer IDS licenses the evaluation software Guardian for its radar devices. The real-time processing was developed with a specific focus on open-pit mines. In these applications, rapid movements of the order of centimetres per day are of particular interest. Guardian filters out slower velocities and becomes sensitive to movement only at higher speeds. In return, the evaluation reacts very quickly to changing deformation rates.

The algorithm does not allow for phase range shifting or phase wrap tracking. It also relies heavily on the measurements' coherence for quality assessment. Hence Guardian does not have the capability to follow fast processes and could not be used for the online monitoring of the Birchgletscher collapse.

Figure 15 and Figure 16 show results from mid-June when the process had slowed down and Guardian could resolve the velocities once again. Figure 15 is a direct output of Guardian. The software allows only for linear colour scaling and therefore the colour coding differs from all other results shown in this report, which cover a much larger velocity range thanks to a logarithmic colour scale.

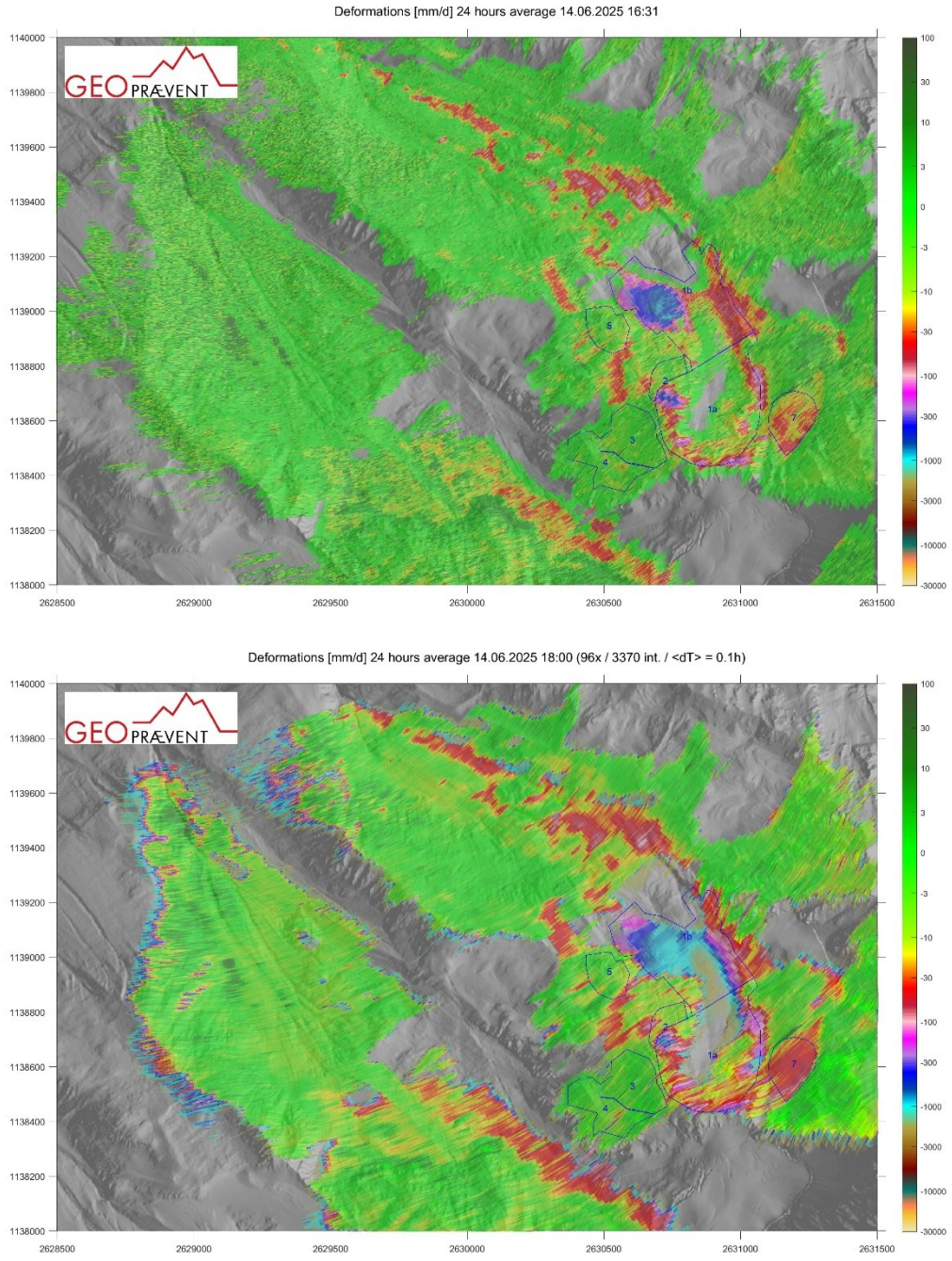


Figure 16: Comparison of the Guardian (upper) and AIM (lower) 24-hour deformations result on 14 June 2025. The results are projected to a hillshade map and use the same colour scale.

Figure 16 shows the same Guardian 24-hour deformation results (upper) and the corresponding AIM aggregate (lower) on a hillshade map with the same colour coding allowing a comparison of the results. The AIM aggregation has a 3x3 median filter applied. Hence areas in motion appear to be larger while transitions are smoother then in the Guardian results. The median filter enhances the reliability of the result by focusing on deformations of a minimal size of the 3x3 pixels, a requirement that also reflects the general handling of the raw data in the AIM algorithm.

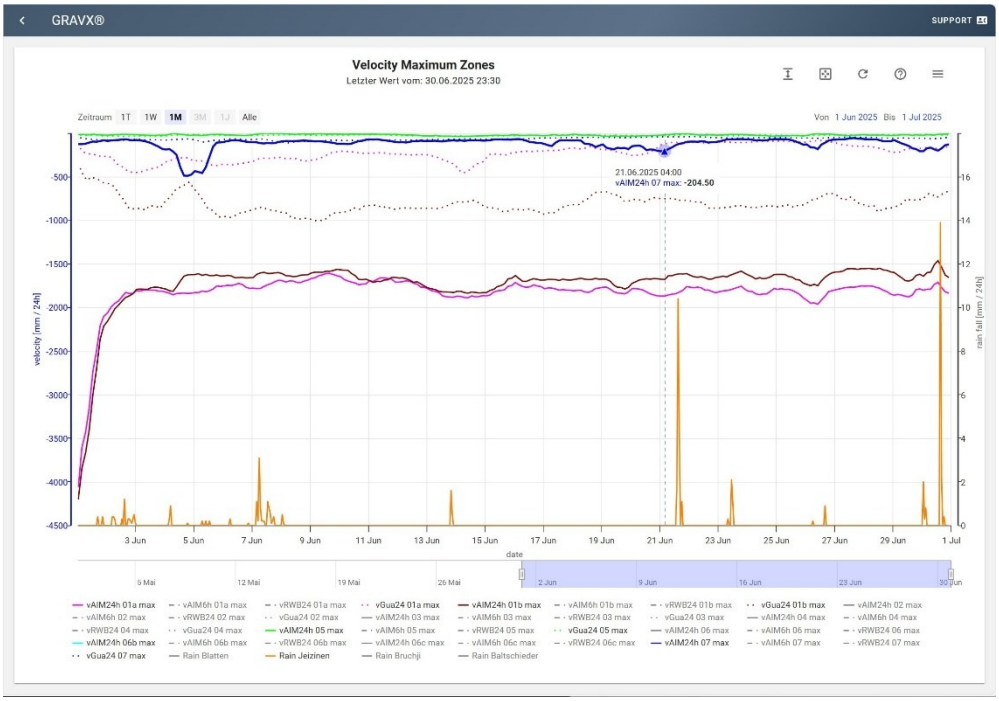


Figure 17: The maxima trends (1st percentiles) of Guardian (dotted) and AIM (solid) 24-hour results are shown for selected ROIs. The orange line represents the daily precipitation levels for the nearby MeteoSwiss station in Jeizinen.

The spatial distributions of the results differ slightly between the two analysis methods. For example, in the distal part of ROI 1b, Guardian shows no movement in green, while AIM, for the same region, no results at all. The reason are different quality criteria. As can be seen in the FlexCam pictures zoomed onto the former Birchgletscher[6] there was still a lot of activity in this region in June: deposits from the east flank still hit the gravel in the bed of the former glacier. Therefore, there is a paucity of available coherent radar results, and the reliability of the radar measurements can hardly be assessed. For such radar pixels AIM does not show any results. Guardian applies apparently different quality criteria, but the area was rarely at rest, as indicated by its results.

On the other hand, AIM shows for the distal walls of the glacier bed velocities of about -1 m/day (Cyan). Coherence in these parts is low, but results are still quite consistent and are therefore deemed reliable. The velocities measured by Guardian are significantly lower in the same areas. This and the results inside of the former glacier bed could be a systematic misinterpretation for such low coherence results on the part of the Guardian algorithm: if too many noisy results are averaged, such random values of a symmetric distribution will introduce a bias towards zero.

This bias can clearly be seen in Figure 17 which pictures selected ROIs' maxima trends, i.e. the first percentiles in the ROIs, for Guardian (dotted) and AIM (solid line) 24-hour results. The differences are most pronounced for ROIs 1a and 1b, for which AIM measured maximal velocities around -1.7 m/d while Guardians indicates lower speeds at -0.8 m/d (ROI 1b) or even -0.2 m/d (ROI 1a).

[6] Blatten 4 Science directory: 02Ab02_GP-FlexCam-Birchbach-p02-Birchgletscher
Geoprevent GRAVX site: https://app.geoprevent.com/stations/640

A similar, but less pronounced difference can be seen for the upper Birchgletscher in ROI 7. In the second week of June the values show similar trends with AIM velocities being about 10% faster than Guardian. On the hot sunny days of the second part of June, AIM shows more daily effects of the glacier melting/freezing than Guardian.

In the stable reference ROI 5 the trends of the maxima in the area are very comparable at values around -20 mm/day. These values are dominated by the resolution achieved by the radar device: the first percentile used for the maxima trends correspond for normal distributed, symmetric data to 2.3 standard deviations of the distribution. Due to the strong thermal effects in the valley and the distance of the target area from the radar device, such a deformation resolution compares well with measurements at other comparable sites.



Figure 18: High resolution image from the ProCam on the east side of Birchgletscher shortly after its installation on 27 May 2025. The time below the logo is in UTC.

13 DEFOX Birchgletscher Deformation Results

A GP ProCam was installed on 27 May 2025 on the east side of the Birchgletscher. The ProCam is a complete system including the camera and all components required for autonomous operation and online access to data and images.

The system is based on a high-quality 42 MP HDR camera with precisely calibrated optics. Cameras are housed in weatherproof enclosures and operate fully automatically with time-controlled image capture. It is designed for continuous use in extreme environments such as glaciers, mountains and even at polar latitudes, delivering high-resolution image data for centimetre-level displacement detection over large areas.

Figure 18 shows one of the first images captured after its installation on 27 May. A precise Zeiss Batis optics with a focal length of 18 mm was used to cover a maximum area despite the very close position of just 100 m adjacent to the former glacier. The image shown is a tone mapped version of the 7952 x 5304 pixels large HDR image.

To ensure consistent image quality, multiple exposures are captured and merged into an HDR image. This enables accurate structure recognition even with strong contrast between sunlight and shadow. The selection of image pairs and the evaluation algorithms play a crucial role in determining analysis quality. HDR processing enhances performance under challenging lighting conditions by increasing contrast. Geoprevent's proprietary algorithms also generate HDR night images, expanding the evaluable area and further improving overall analysis quality.

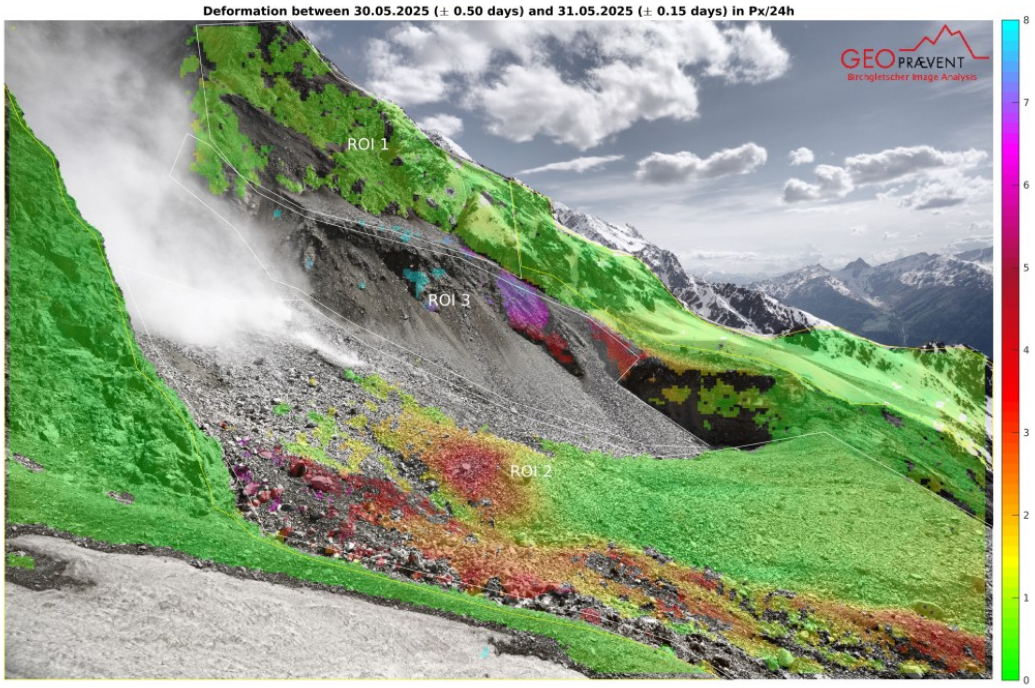


Figure 19: The DEFOX deformation result for the bed of the former Birchgletscher shortly after the collapse. The deformations are measured in camera pixels per day, small arrows inside the pixels indicate the direction of the movement.

The ProCam camera system enables precise analysis of movement processes within monitored areas. To support this, Geoprevent has developed the DEFOX deformation analysis method, which uses the ProCam optical data to measure the displacement of small image segments in the two deformation components perpendicular to the viewing direction. Suitable image pairs are automatically selected, registered and correlated in 25x25 pixel patches of the images.

For the time before the collapse the velocities were too high and the changes of the surface of the glacier too severe for the DEFOX algorithm to calculate a reasonable deformation result. Figure 19 shows a DEFOX deformation results between 30 and 31 May. The deformation rates are colour coded and the deformation movements are shown by small arrows inside the pixels. Areas considered stable are marked with yellow, ROIs with white lines.

On the right side of the picture the bed of the former glacier has slowed down to rates 1-2 pixels per day (right part of ROI 2). Towards the camera position movements of the order of 4-6 pixels/day are measured. On the left side of ROI 2 a lot of debris from the east flank of Kleines Nesthorn distorts the surface continuously and renders an image-based deformation analysis impossible. Therefor no results are shown for this area. The walls of the glacier bed in ROI 3 are still too unstable to yield continuous deformation results and therefore only few pixels show high rates (cyan and purple). The north flank of the Kleines Nesthorn in ROI 1 does not show significant deformations (green).

Table 1: Camera parameters for the ProCam Birchgletscher at the time of the collapse determined with the DEM recorded by TERRADATA on 23 May 2025.

Camera position CH1903+ / LV95	2630838.93, 1139382.70, 2700
Camera orientation:	216.73° N
Camera elevation:	-16.35°
Camera tile	-0.61°
Lens opening angles	89.4° x 59.6°

To transform the resulting deformations from pixels to metric units, the exact position and orientation of the camera needed to be georeferenced. This was done a posteriori with a drone scan performed by TERRADATA on 23 May 2025. About 20 reference points were identified on the camera picture and the orthophoto of the scan with their exact positions on the TERRADATA DEM. With the help of these reference points the orientation was determined as noted in Table 1.

The movement of the glacier on 27 and 28 May 2025 can be estimated by tracking features on consecutive images. In Figure 20 and Figure 21 the method is demonstrated on an example feature in the centre of the images. The two images taken on 27 May were captured within 1 hour. The leading edge of the rock measured moved about 25 camera pixels within this hour.

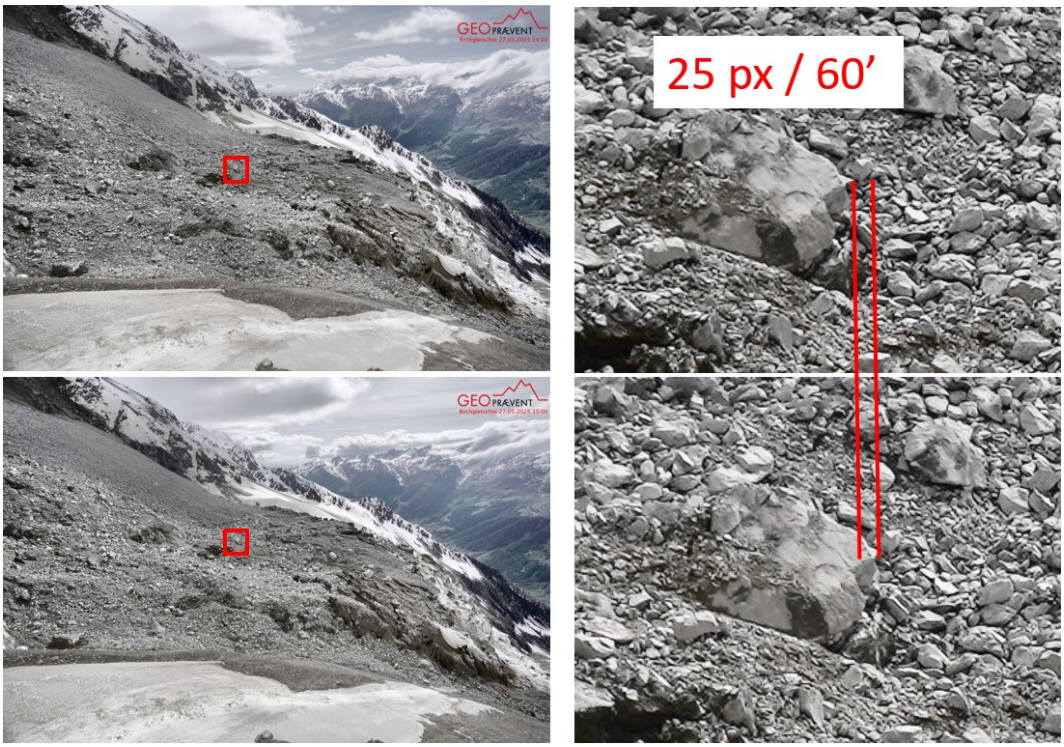


Figure 20: Two consecutive HDR images of the Birchgletscher DEFOX camera on 27 May 2025, at 2pm and 3pm (left) and detail zoom within the red box in the right column. The edge of the rock moved by 25 camera pixels within the hour.

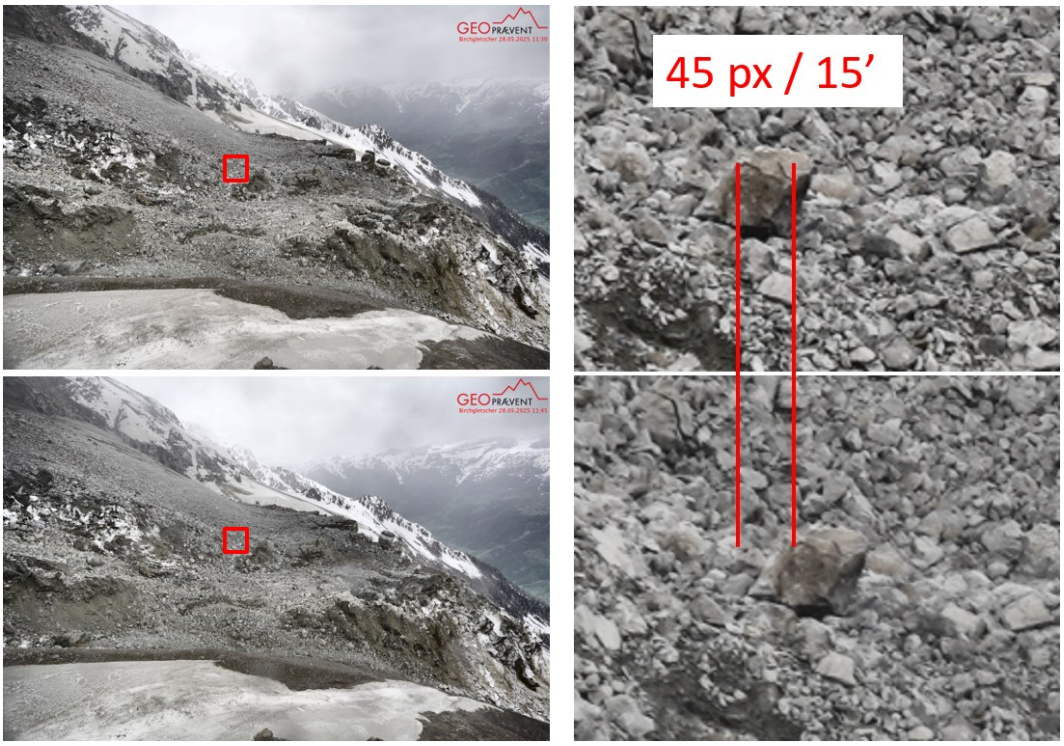


Figure 21: Two consecutive HDR images of the Birchgletscher DEFOX camera on 28 May 2025, at 11:30am and 11:45am (left) and detail zoom within the red box in the right column. The edge of the rock moved by 45 camera pixels within the 15’ period.

On 28 May the frequency of the image capturing was increased to four pictures/hour. The rock measured in Figure 21 travelled 45 camera pixels between the two pictures taken 15 minutes apart. That means that the velocity has increased by more than a factor of seven in the 21 hours between the analysed image pairs.

Appendix A Birchgletscher Collapse FlexCam Still Frames

Figure 22, Figure 23 and Figure 24 show still frames from a video clip taken with the Geoprevent FlexCam during the collapse of the Birchgletscher. The FlexCam is situated on the other side of the valley at Weritzstaffel in about 3.7 km distance from the former Birchgletscher front. The FlexCam has good pan, tilt and zoom capabilities and can be operated manually by users of the Geoprevent GRAVX portal. Such a manipulation actually happened during the collapse: the zoom level and camera orientation changed on 28 May after 15:24:27 CEST. The last still frames before that intervention are shown in the figures to illustrate the first moments of the Birchgletscher collapse from this perspective.

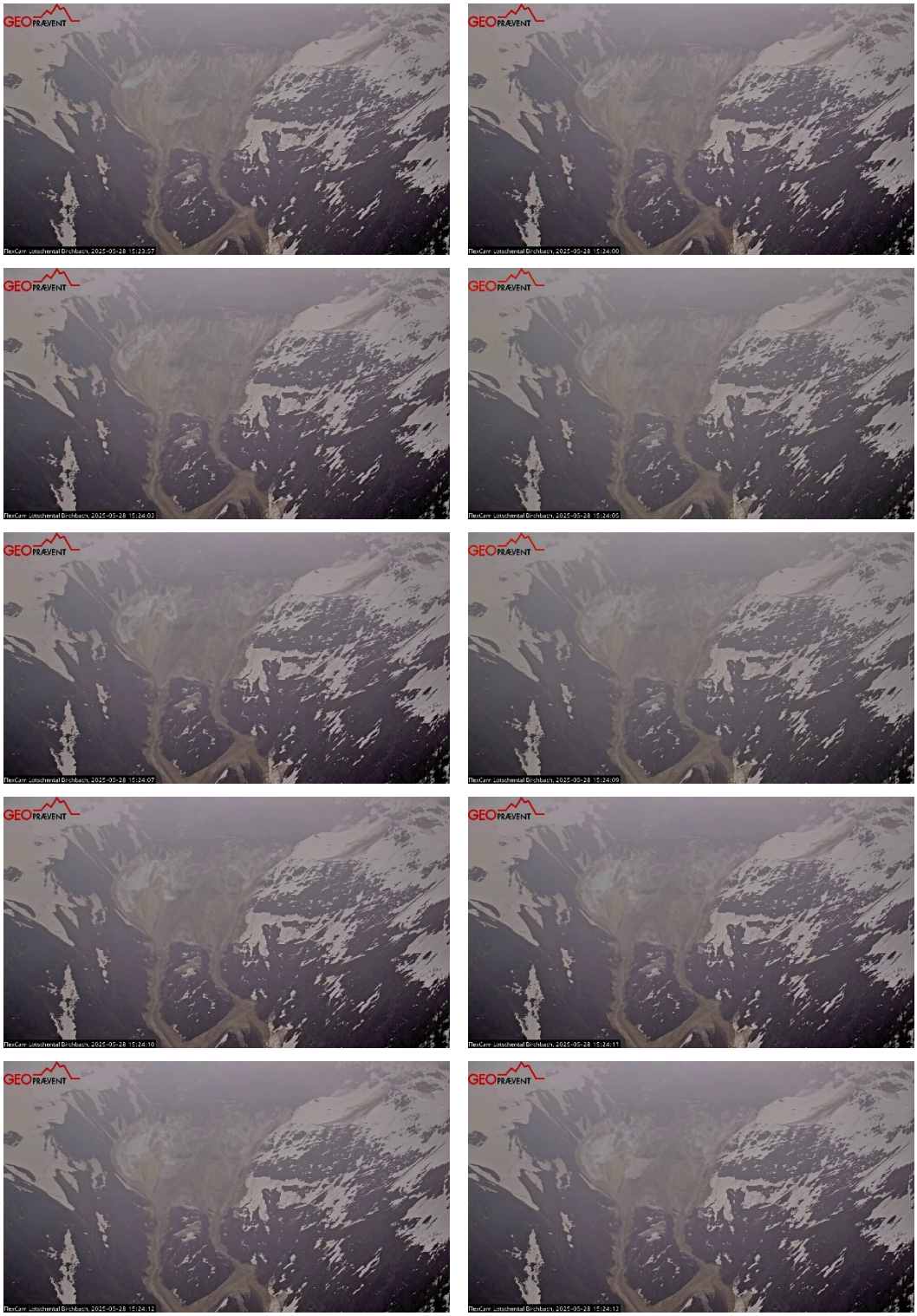


Figure 22: Still frame images from Birchbach FlexCam at Weritzstaffel immediately before the Birchgletscher collapse 28 May 2025 from 15:23:57 to 15:24:13.

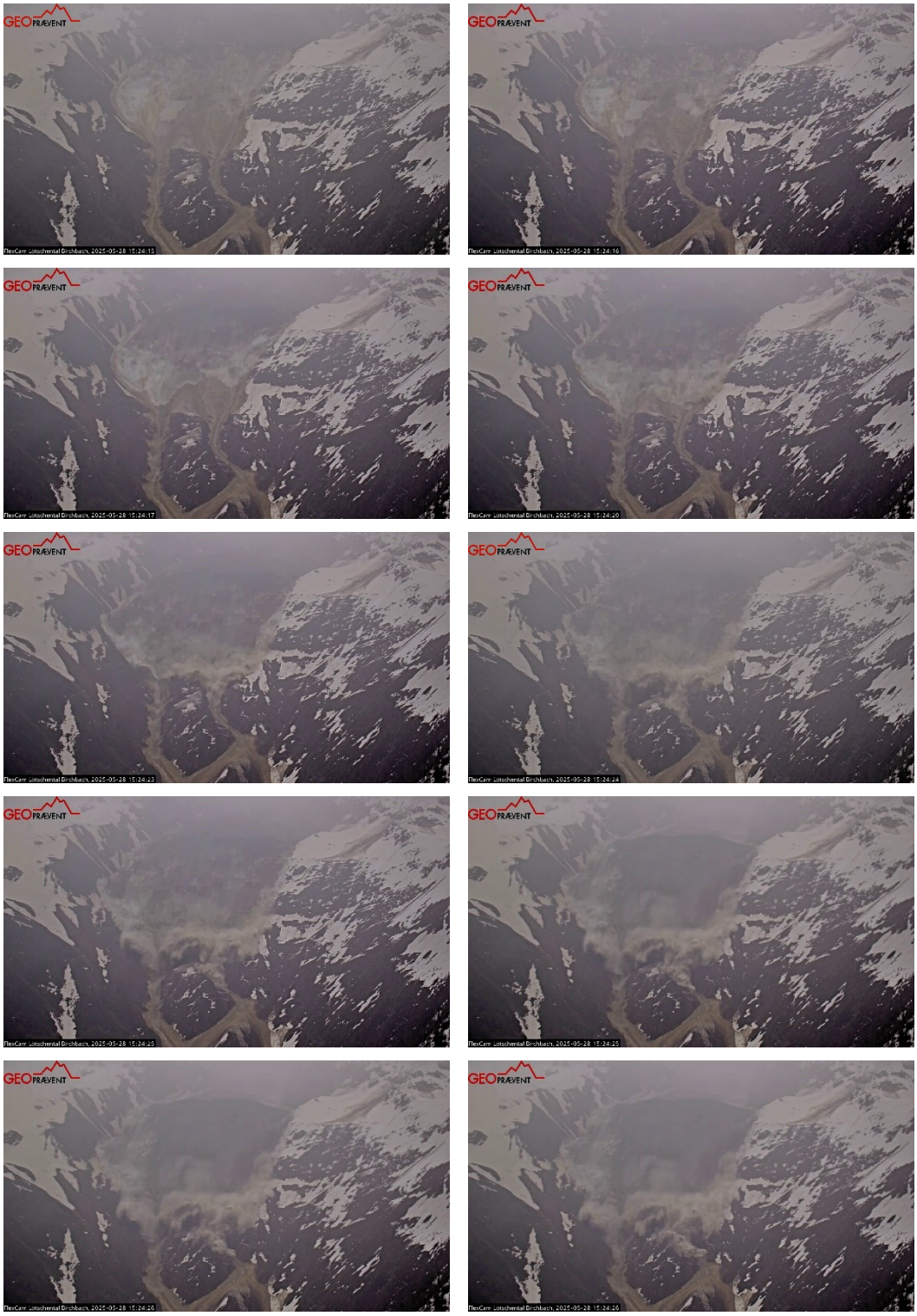


Figure 23: Still frame images from Birchbach FlexCam at Weritzstaffel immediately before the Birchgletscher collapse 28 May 2025 from 15:24:15 to 15:24:26.



Figure 24: Still frame images from Birchbach FlexCam at Weritzstaffel immediately before the Birchgletscher collapse 28 May 2025 from 15:24:26 to 15:24:27.

Appendix B Overview Images on Target Area

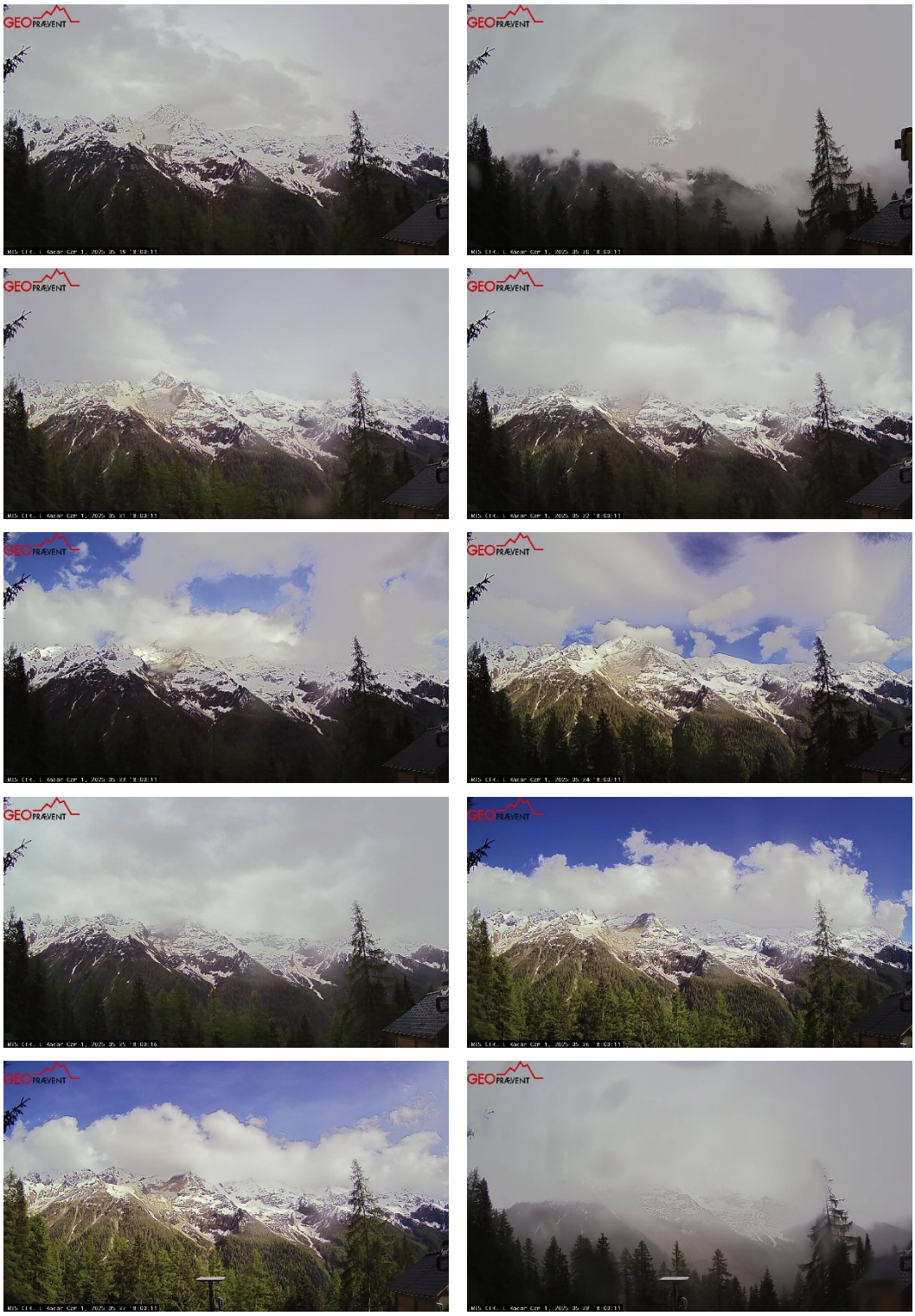


Figure 25: Daily overview Images from the radar station cam at 6pm local time between installation on 19 May and the Birchgletscher collapse on 28 May 2025.

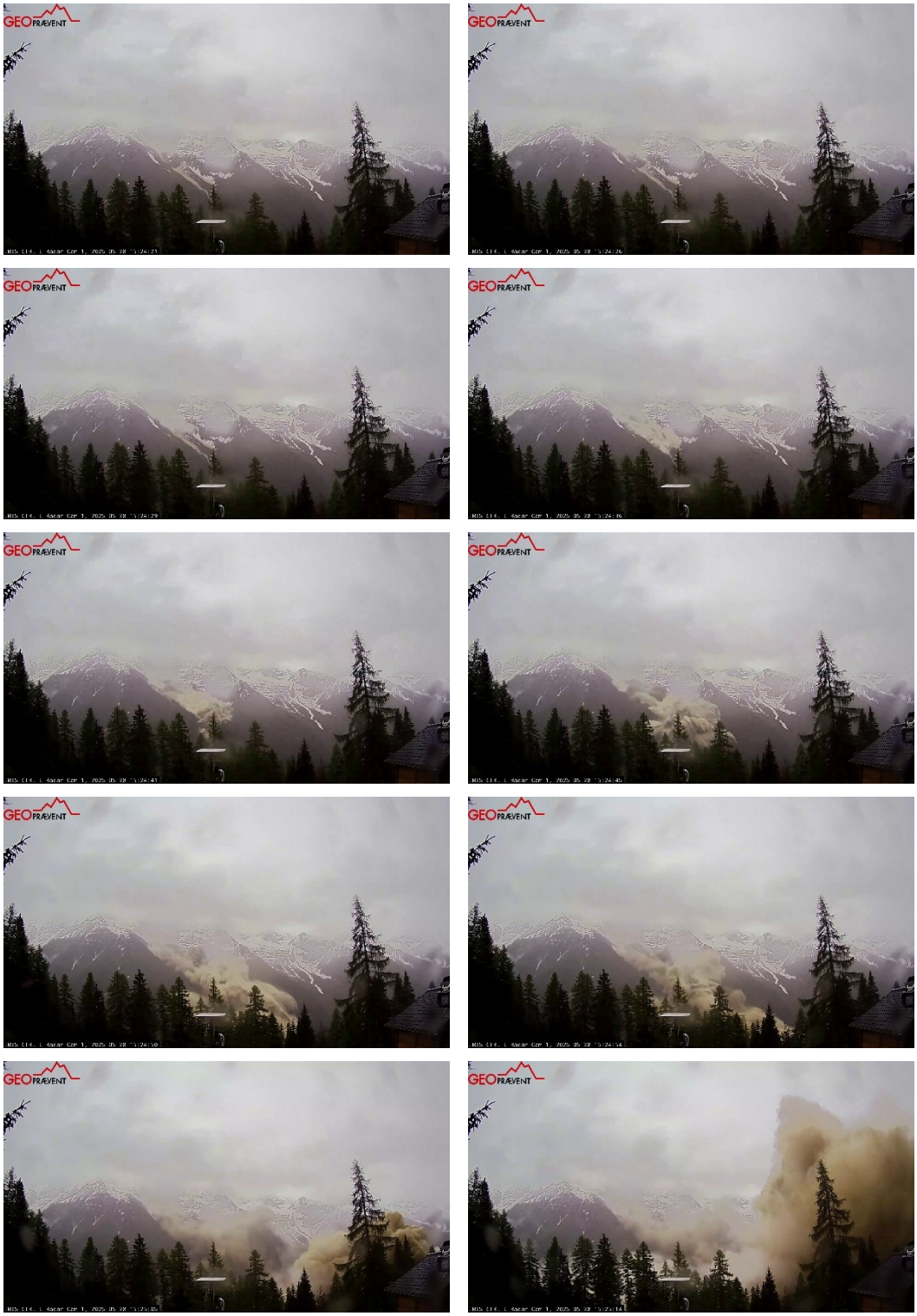


Figure 26: Still frame images from the radar station camera during the collapse of the Birchgletscher 28 May 2025 from 15:24:21 to 15:25:20.

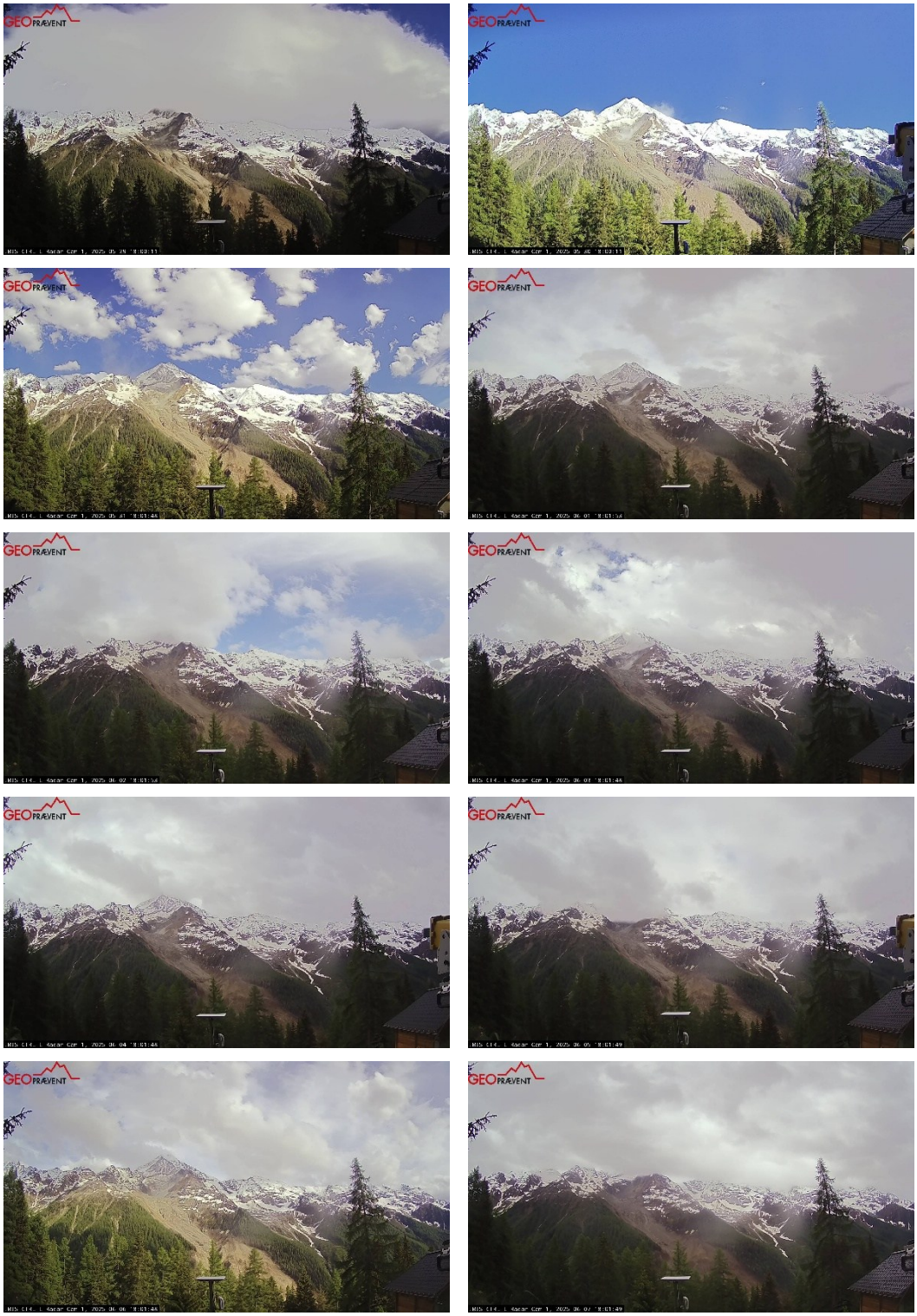


Figure 27: Daily overview Images from the radar station cam at 6pm local time after the collapse between 29 May and 7 June 2025.

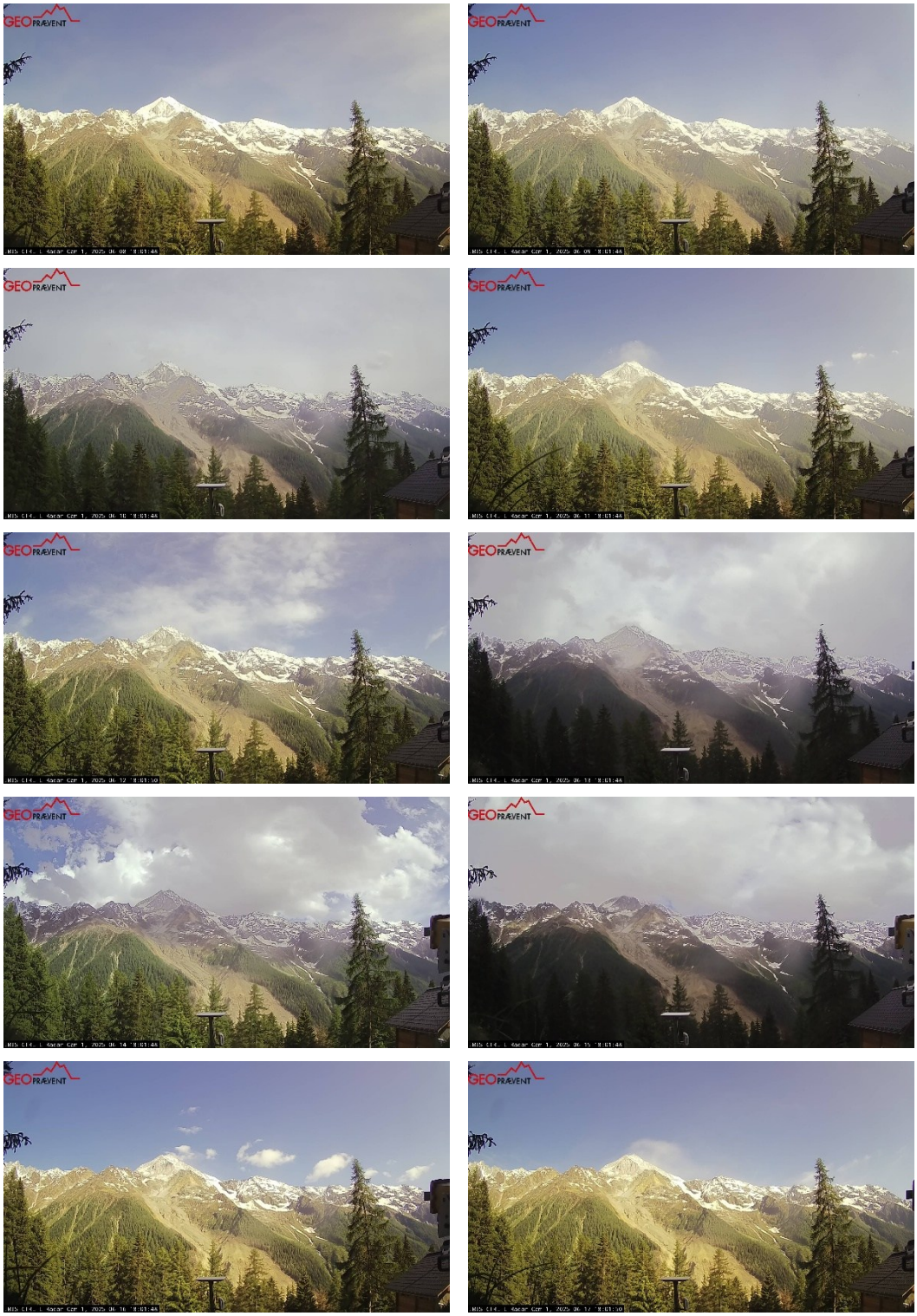


Figure 28: Daily overview Images from the radar station cam at 6pm local time after the collapse between 8 and 17 June 2025.

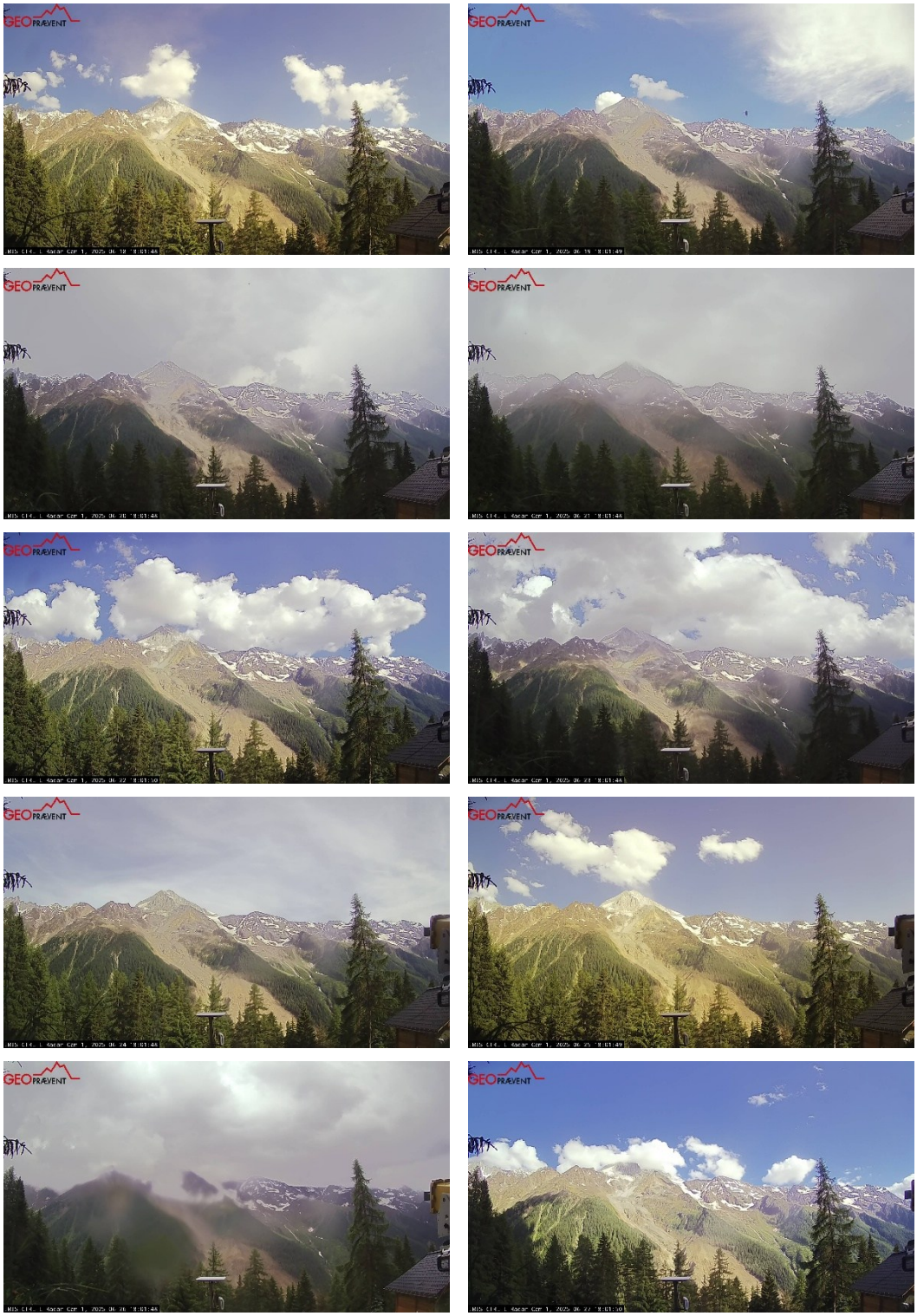


Figure 29: Daily overview Images from the radar station cam at 6pm local time after the collapse between 18 and 27 June 2025.

Appendix C Interferograms and Coherence Maps

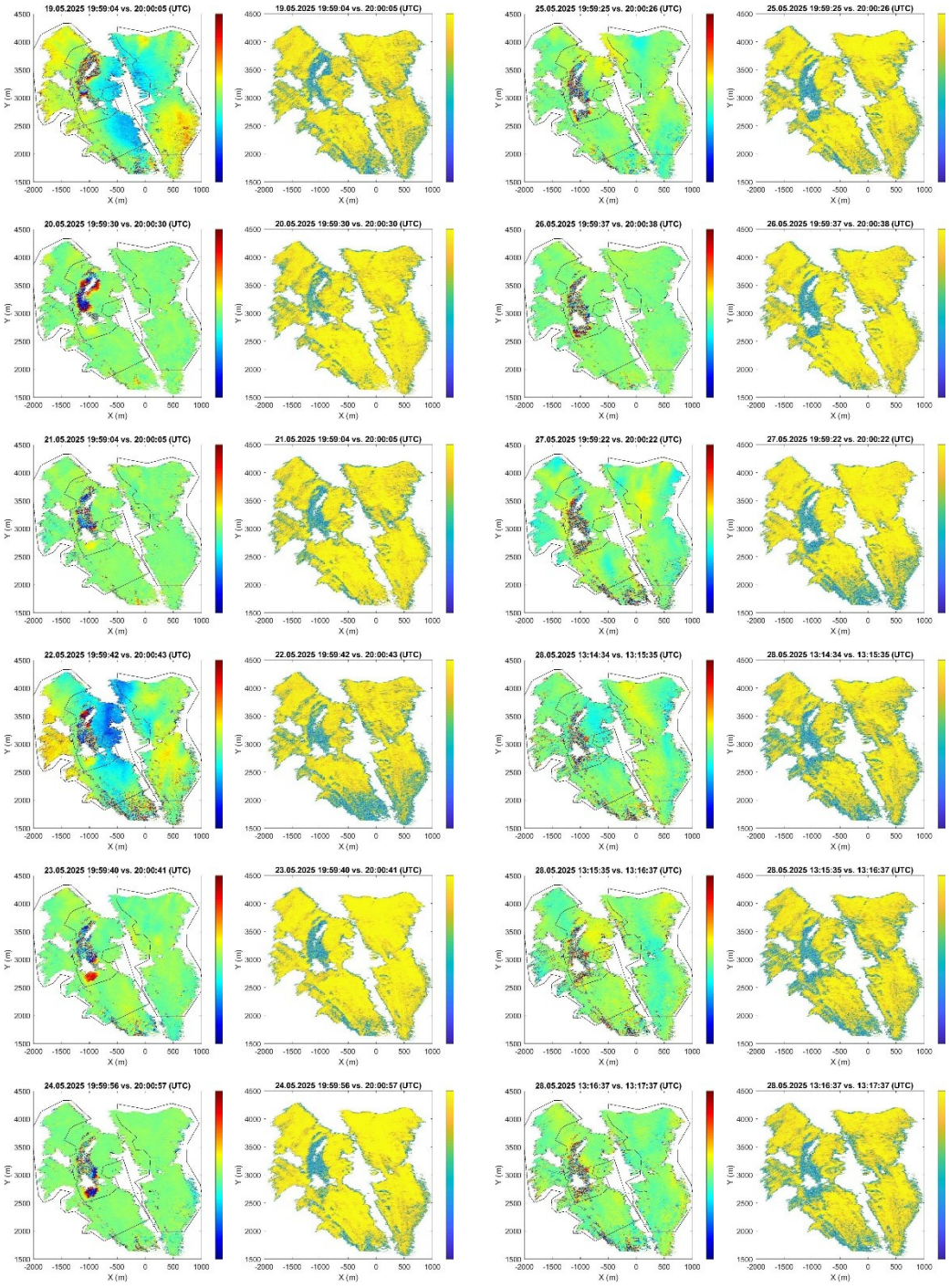


Figure 30: Interferograms (1st & 3rd column) and coherence maps (2nd & 4th column) of consecutive scans during phase 2 from 19 to 28 May 2025.

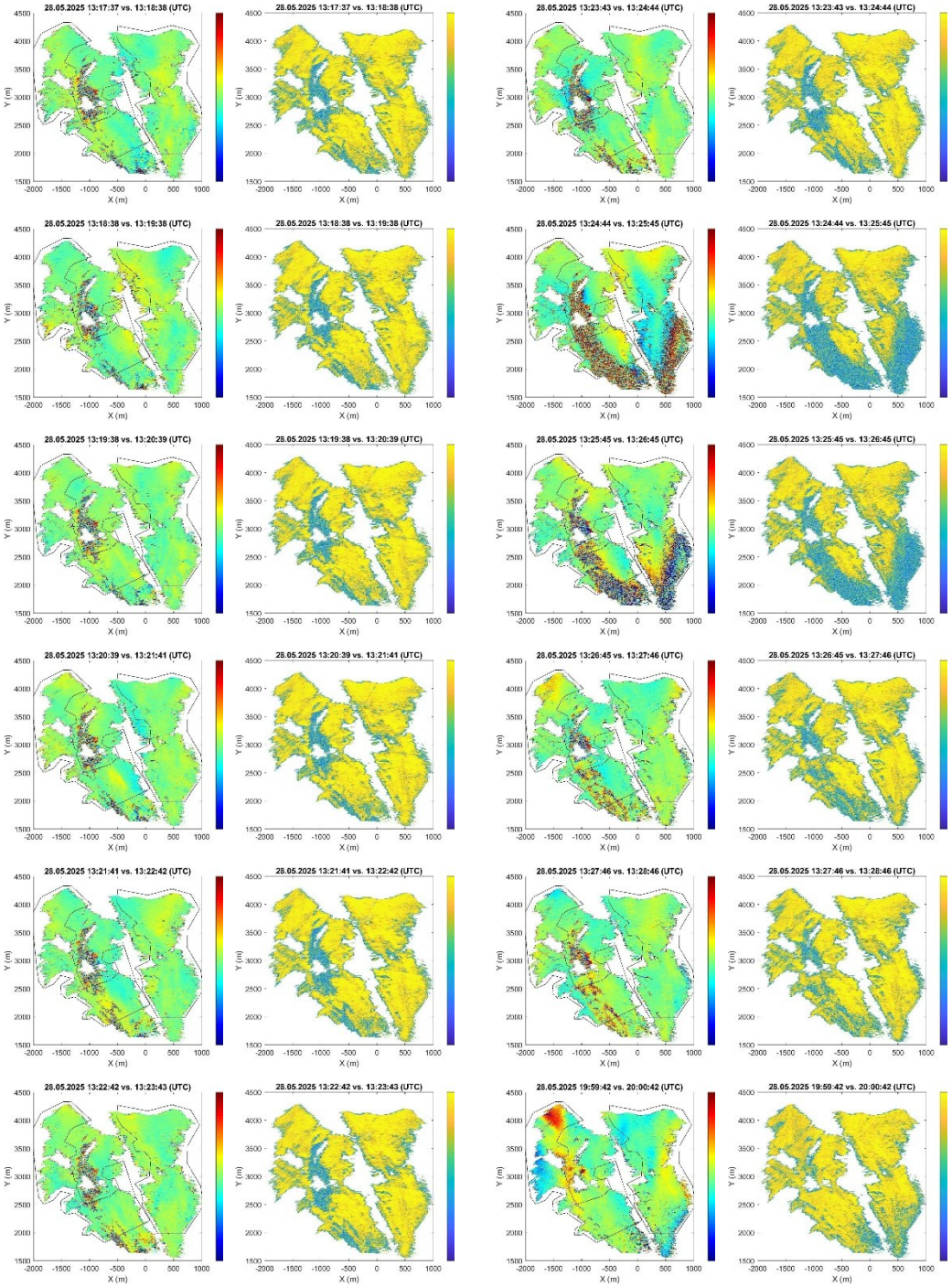


Figure 31: Interferograms (1st & 3rd column) and coherence maps (2nd & 4th column) of consecutive scans during the collapse on 28 May 2025.